Ore Geology Reviews 150 (2022) 105160

Contents lists available at ScienceDirect

Ore Geology Reviews

journal homepage: www.elsevier.com/locate/oregeorev

Provenance of Late Permian Nb-Zr-REE-Ga enrichment in western Guizhou: Implications for the waning volcanism of Emeishan large igneous province

Wei Deng [a,c], Han-Jie Wen [b,c,*], Sheng-Jiang Du [d], Kun-Yue Ling [a], Hai-Feng Fan [a], Chuan-Wei Zhu [a], Chong-Guang Luo [a], Yang Yang [a]

[a] State Key Laboratory of Ore Deposit Geochemistry, Institute of Geochemistry, Chinese Academy of Sciences, Guiyang 550081, China
[b] School of Earth Science and Resources, Chang'an University, Xi'an 710054, China
[c] University of Chinese Academy of Sciences, Beijing 100049, China
[d] State Key Laboratory of Nuclear Resources and Environment, East China University of Technology, Nanchang 330013, China

ARTICLE INFO

Keywords:
Critical metals
Xuanwei formation
Zircon U−Pb age
Zircon Hf isotopes
Alkaline magmatism
Emeishan large igneous province

ABSTRACT

Nb-Zr-REE-Ga-enriched beds are widely found in the Late Permian clastic sediments in southwestern China and are related to the Emeishan large igneous province (LIP). To determine the provenance of these beds, we analyzed their geochemical and mineralogical compositions, along with zircon U−Pb ages, Hf isotopes, and trace elements. Our data show that these polymetallic beds have high Al_2O_3 contents, Al_2O_3/TiO_2 (e.g., mostly >8) and Th/Sc (e.g., mostly >0.6) ratios, low Fe_2O_3, TiO_2 contents, and Ti/Y ratios (e.g., mostly <500). These beds exhibit strong negative Ti, Eu, and Ba anomalies, positive HFSEs (high field strength elements) and REEs (rare earth elements) anomalies in trace element patterns, and show geochemical affinities with the alkaline silicic rocks at the top of the Emeishan lavas. Zircons from the polymetallic beds yield U−Pb ages of 259.2–256.2 Ma and $\varepsilon Hf(t)$ values of −10.1 − +13.4, which are consistent with the zircon data of the alkaline rhyolites. These results suggest that the mineralized beds dominantly derived from the waning Emeishan silicic volcanism, whereas the barren samples have mixed basaltic compositions. The primary rutile was associated with low-temperature zircon, and was replaced by Nb-rutile and columbite, which were likely to crystallize from an alkaline magma that experienced hydrothermal process. Additionally, the temporal decreases of zircon Eu/Eu* values and crystallization temperatures indicate that rare metals were enriched during the protracted alkaline magmatism. The zircons from the older samples show higher Th/Nb, U/Yb ratios and more negative $\varepsilon Hf(t)$ values than those from the younger samples, suggesting that the eroded source rocks were generated by waning silicic volcanism with decreasing crustal assimilation.

1. Introduction

The Nb(Ta)-Zr(Hf)-REY(rare earth element and yttrium)-Ga mineralization in the clastic sediments of coal basin was widely reported and attracted much attention (Seredin and Finkelman, 2008; Seredin and Dai, 2012; Dai et al., 2016a; Arbuzov et al., 2019; Zhao et al., 2019). In southwestern China, the polymetallic beds were mainly developed in the Upper Permian coal-bearing Xuanwei Formation in eastern Yunnan and western Guizhou (Dai et al., 2010, 2014; Zhang et al., 2016; Zhao et al., 2016), as well as in the synchronous Longtan Formation in western Guizhou, northeastern Yunnan, and southeastern Sichuan (Dai et al., 2016b; Liu et al., 2019; Shen et al., 2021; Wang et al., 2022). Prior to the study of this mineralization, the Nb-Zr-REE-rich kaolinic mudstones in the coalfield of eastern Yunnan were identified as tonsteins that formed due to the alteration of airborne volcanic ashes (Zhou et al., 1982, 2000; Burger et al., 1990). Combined with well logging data, a new type of Nb-Zr-REE(rare earth element)-Ga deposit was reported in these tonsteins, which was derived from the alkaline pyroclastics of the Emeishan large igneous province (LIP; Dai et al., 2010).

A model of mineralization suggested that the rare metal-enriched tonsteins in eastern Yunnan were originated from alkaline volcanic ashes and pyroclastics, followed by continuous hydrothermal-weathering processes (Zhao et al., 2016, 2017; Dai et al., 2018). Different from these tonsteins, the mineralogical characteristics of the

* Corresponding author at: State Key Laboratory of Ore Deposit Geochemistry, Institute of Geochemistry, Chinese Academy of Sciences, 99th West Lincheng Road, Guiyang, Guizhou Province, China.
E-mail address: wenhanjie@vip.gyig.ac.cn (H.-J. Wen).

https://doi.org/10.1016/j.oregeorev.2022.105160
Received 30 May 2022; Received in revised form 9 October 2022; Accepted 14 October 2022
Available online 17 October 2022

polymetallic coals, tonsteins, and K-bentonites from western Guizhou and southeastern Sichuan suggest a terrigenous source of intermediate-felsic rocks in the Emeishan LIP (Dai et al., 2016b; Liu et al., 2019; Shen et al., 2021). However, the studies of the REE enrichment in these polymetallic beds proposed that they were generated from the weathering crust of the underlying basalts (Huang, 1997; Yang et al., 2008). Further works suggested that these REE-enriched layers (also rich in Nb, Zr, and Ga) were mainly derived from the Emeishan basalts and were controlled by the transportation and deposition of weathered materials (Zhang et al., 2010, 2016; Zhou et al., 2013). Therefore, the provenance of the polymetallic beds needs further constraints and the mineralization model is still being discussed.

The zircon geochronology data suggest that the lowest member of the Xuanwei Formation at the periphery of the Chuandian old land is temporally consistent with the late-stage volcanism of the Emeishan LIP (Fig. 1; He et al., 2007; Meng et al., 2015; Huang et al., 2016). Based on stratigraphic correlation, the clastic sediments in the lower Xuanwei Formation are proposed to have unroofed from the silicic rocks at the top of the Emeishan volcanic sequence (He et al., 2007, 2010; Xu et al., 2010). Nevertheless, the basaltic tuff, tuffaceous clay, and iron ore bed in the lower Xuanwei Formation are weathered from the underlying basalts (Meng et al., 2015; Zhang et al., 2016). Thus, the correlation between the sedimentary succession of the Xuanwei Formation and the Emeishan volcanic sequence remains a detailed study. The zircon U−Pb ages and Hf isotopes from the correlative sediments in coeval Longtan and Shaiwa formations indicate that the pre-erosional source rocks are dominantly generated from the silicic volcanism of the Emeishan LIP (Yang et al., 2015; Deng et al., 2020). But the zircon U−Pb ages, Hf isotopes, and trace elements from the polymetallic beds are lacking, and the lithologic components and magmatic evolution of their source rocks need a deeper understanding.

In this study, we conducted comprehensive provenance research on the Nb-Zr-REE-Ga enrichment in western Guizhou Province. Whole-rock geochemical and mineralogical compositions, along with zircon U−Pb geochronology, enabled us to determine their possible source. Meanwhile, our new zircon Hf isotopes and trace elements are used to understand the generation of the eroded volcanic rocks of the Emeishan LIP. This study provides new insights into the metallogenic processes of the polymetallic enrichment in western Guizhou. Examination of the lower Xuanwei Formation also helps us to reveal the evolution and mineralization of the waning Emeishan volcanisms.

2. Geological setting

The Emeishan LIP in southwestern China and northern Vietnam covers an area of ~0.3×10^6 km^2 (Chung and Jahn, 1995; Xu et al., 2001, 2004; Shellnutt, 2014), and further studies have extended this area up to ~0.7×10^6 km^2 (Usuki et al., 2015; Li et al., 2017; Liu et al., 2017). Based on the extent of erosion of the underlying Maokou limestone, the Emeishan LIP was divided into inner, intermediate, and outer zones

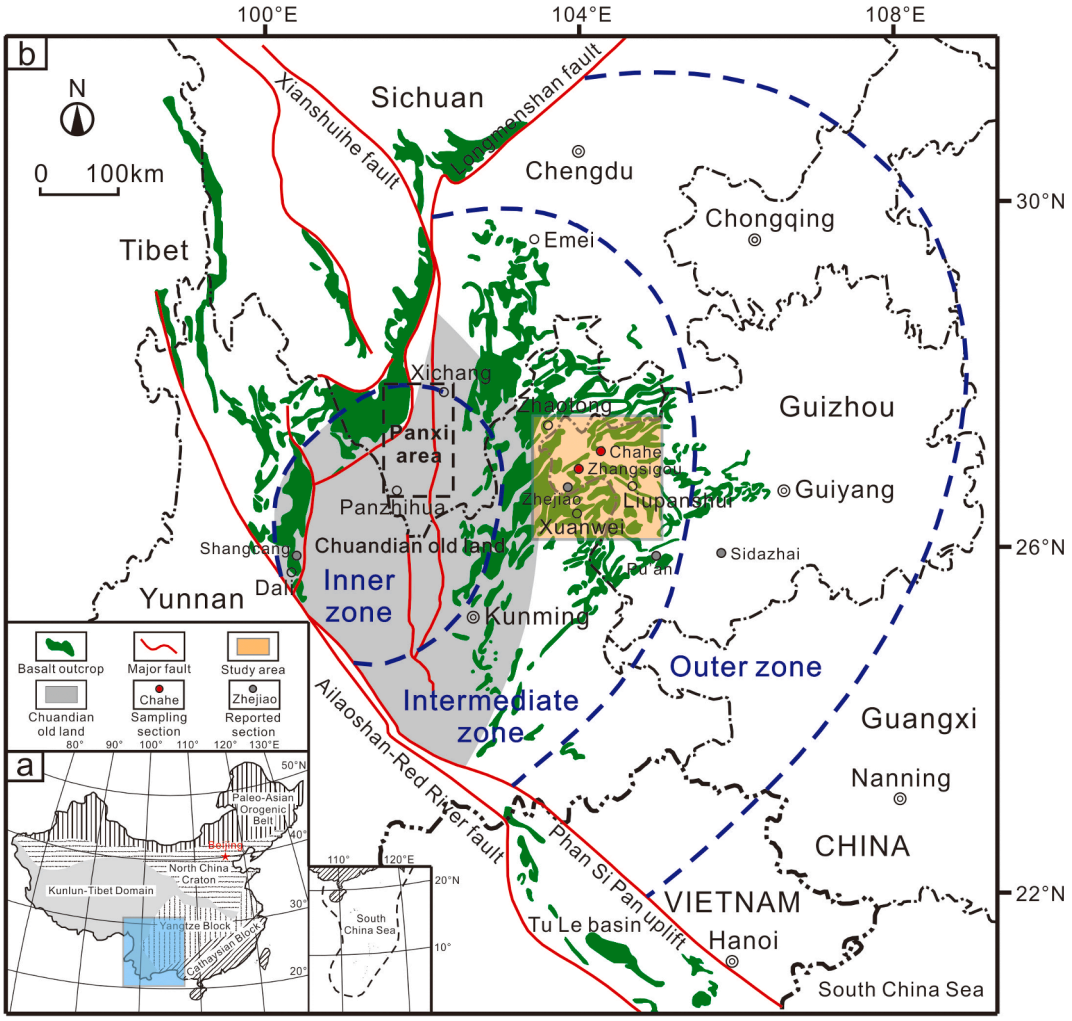

Fig. 1. Schematic map of the Emeishan flood basalts and the study area (modified after He et al., 2007; Shellnutt, 2014). Dashed lines separate the inner, intermediate, and outer zones of the Emeishan large igneous province (LIP; He et al., 2003). The sampling sections are denoted in red points.

(Fig. 1; He et al., 2003). The thickness of the volcanic sequence varies from >5000 m in the western inner zone to several hundred meters in the eastern outer zone (Xu et al., 2001; He et al., 2003). The Emeishan LIP consists of voluminous basalts, picrites, ultramafic-mafic intrusions, felsic plutons, and silicic rocks at the top of the volcanic sequence (Chung et al., 1998; Xu et al., 2001, 2010; Xiao et al., 2004; Shellnutt, 2014; Shellnutt et al., 2020). The plume-induced uplift of the Chuandian old land shaped an erosional region, and the succession of voluminous flood basalts in the central Emeishan LIP was preserved until the Late Triassic (He et al., 2007, 2010).

Soon after the Emeishan LIP eruptions, these volcanic rocks experienced extensive tropical erosion (Xu et al., 2001, 2004), and voluminous amounts of volcanic detritus were input into the adjacent basin during Late Permian (He et al., 2007, 2010; Yang et al., 2014). A sedimentary system has been established by correlating the eroded volcanic rocks with the terrestrial (Xuanwei Formation), littoral (Longtan Formation), and offshore (Shaiwa and Wujiaping formations) successions from western Guizhou to northern Youjiang Basin (He et al., 2007; Zhang et al., 2010; Yang et al., 2015, 2018; Yu et al., 2016; Deng et al., 2020). The Xuanwei Formation, with a thickness of 78–286 m and average thickness of ~200 m, was distributed systematically along the periphery of the Chuandian old land in the central Emeishan LIP (He et al., 2003; Xu et al., 2004). The terrigenous sediments of the Xuanwei Formation were mainly sourced from the west Chuandian old land, which was dominantly composed of Emeishan volcanic rocks (Zhou et al., 1982; Wang and Yin, 2001; He et al., 2007; Zhang et al., 2010). Notably, the silicic rocks at the top of the Emeishan lavas served as a persistent source for the Late Permian sediments at the periphery of the Emeishan LIP (He et al., 2007, 2010; Yang et al., 2015, 2018; Huang et al., 2016; Deng et al., 2020).

The study area is located in western Guizhou Province and belongs to the intermediate zone of the Emeishan LIP (Fig. 1). In this region, the Late Permian terrestrial (Xuanwei Formation) and transitional (Longtan Formation) successions were deposited on the Emeishan basalts and distributed continuously from eastern Yunnan to western Guizhou (Fig. 2). The thick-bedded sandstones of the Lower Triassic Feixianguan Formation conformably overlie the Xuanwei and Longtan formations (Wang and Yin, 2001; Zhang et al., 2010). The Xuanwei Formation is composed of terrigenous clastic sediments, including tuffaceous clays at the bottom, mudstones with interlayered carbonaceous shales or coal seams, bauxitic clay rocks, mudstones interbedded with medium-thick layers of siltstones, and sandstones (Wang and Yin, 2001; He et al., 2007; Zhang et al., 2016). The underlying Emeishan basalts are characterized by tholeiitic and minor alkaline basalts in the lower part, along with basaltic breccia deposited over the flood basalts (Xu et al., 2004; He et al., 2007).

3. Sampling and petrography

The Zhangsigou and Chahe sections in western Guizhou were chosen for this study due to the continuous succession of the Xuanwei Formation and widespread Nb-Zr-REE-Ga mineralization (Zhou et al., 2013; Zhang et al., 2016). The Zhangsigou section is located northwest of Heishitou town, Weining County, and the sampling site is located on the

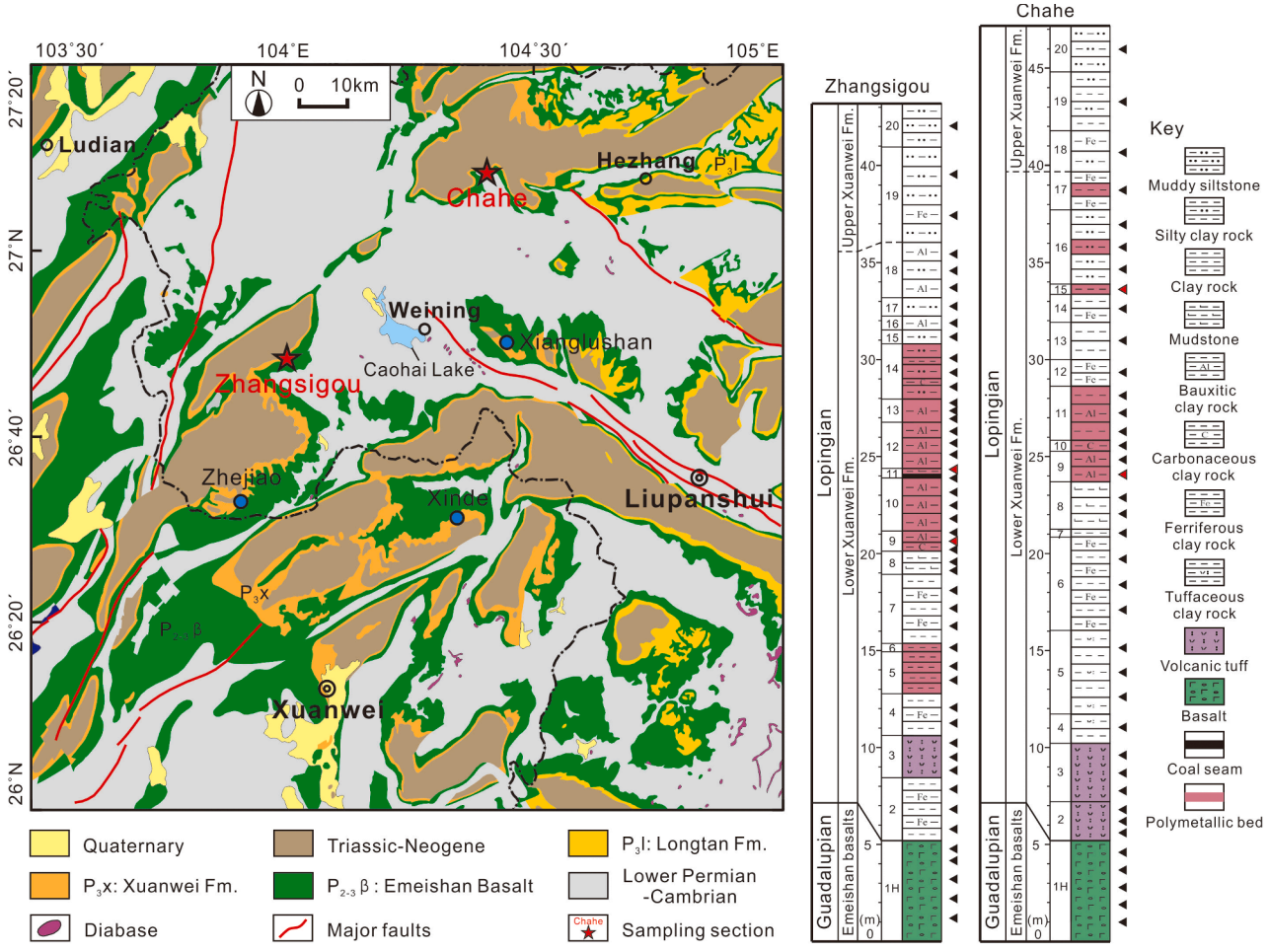

Fig. 2. Simplified geological map and the lithological column of the Zhangsigou and Chahe sections. The Zhejiao (He et al., 2007), Xinde (Dai et al., 2014), and Xianglushan (Meng et al., 2015) sections in this area are denoted in blue points.

eastern side of the Halahe syncline (Fig. 2), which has a dip direction of 345° and dip angle of 30° (Fig. 3a). The Emeishan basalts and the overlying Xuanwei Formation are in unconformable contact. The Chahe section is located in Chahe village, Hezhang County, and the sampling site is located on the southeastern side of the Yangjie syncline (Fig. 2). The Xuanwei Formation outcrops with a dip direction of 350° and dip angle of 15°, which unconformably overlies the Emeishan basalts, with a purplish-red tuffaceous layer (~5 m) deposited between them (Fig. 3b).

Eighty-five samples were collected from the Zhangsigou and Chahe sections, which consist of the Emeishan basalts and Xuanwei Formation

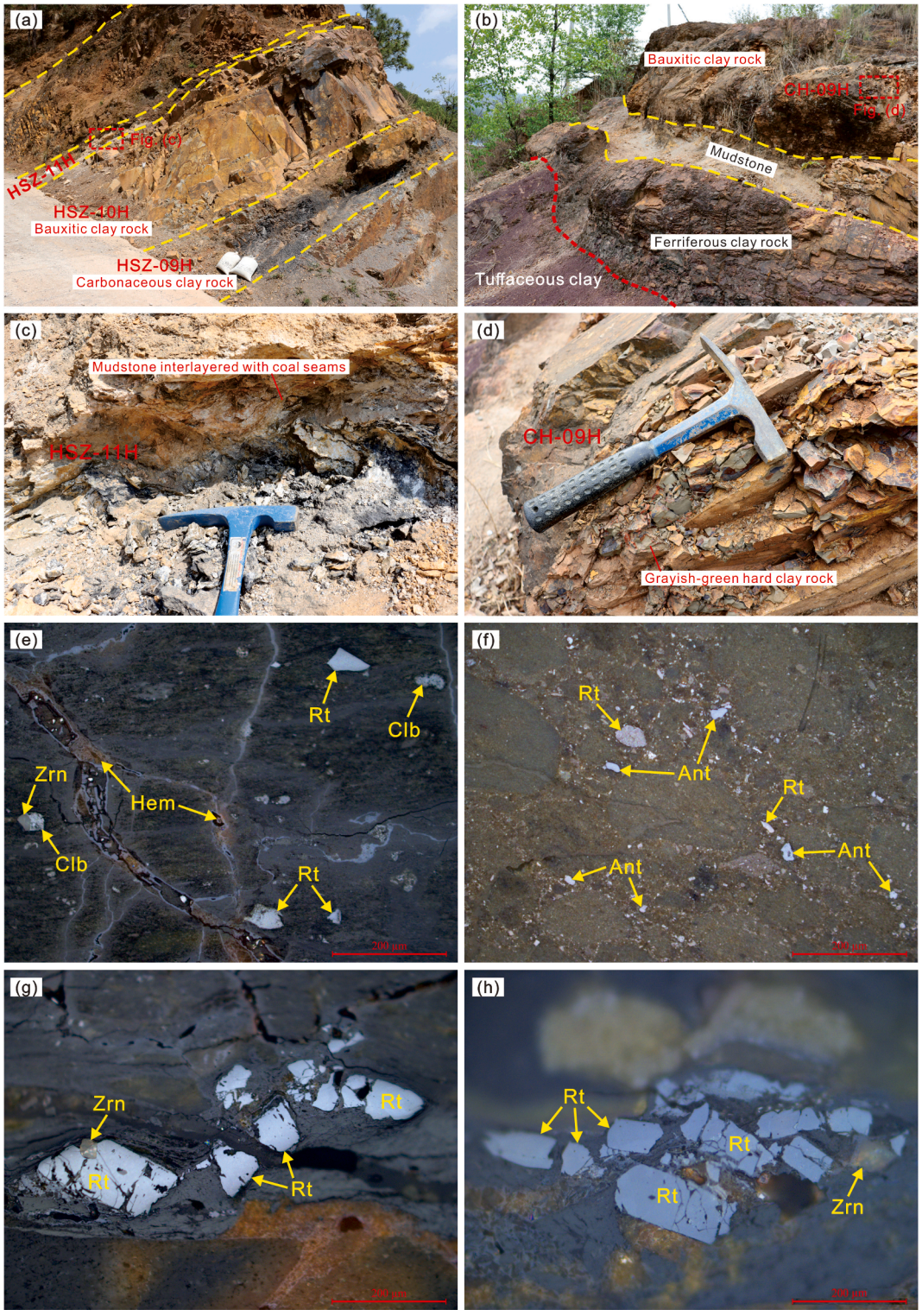

Fig. 3. Representative field outcrops and microphotographs of the polymetallic beds. (a) Mineralized clay rocks in the Zhangsigou section; (b) Tuffaceous clay, ferriferous clay, mudstones, and mineralized clay rocks (from bottom to top) in the Chahe section; (c) Mineralized mudstone interlayered with coal seams in the Zhangsigou section; (d) Mineralized bauxitic clay rock in the Chahe section; (e) Rutile (Rt), columbite (Col), zircon (Zrn), and hematite (Hem) veins in HSZ-11H horizon, plane-polarized light (PPL) under optical microscope; (f) Rt and Anatase (Ant) in CH-09H horizon, PPL; (g) Oriented Rt with Zrn inclusions in HSZ-11H horizon, PPL; (h) Oriented Rt and Zrn in HSZ-12H horizon, PPL.

from bottom to top (Fig. 2). The amygdaloidal basalts at the bottom of sections are black and dark green with vesicular structures, and pervasive chloritization and zeolitization are observed in the fissures and voids. Basaltic debris and purplish-red tuffs overlie the massive basalts, with tuffaceous clays piled on the tuff layers. The volcanic tuff at the bottom of the Xuanwei Formation contains basaltic clastics and varies in thickness (e.g., 1–10 m). The lower part of the Xuanwei Formation is composed of gray kaolinic mudstones, grayish-green hard clay rocks, and thin mudstone layers interbedded with carbonaceous shales or coal seams (Fig. 3a–d), while the upper part is dominated by yellowish-brown silty clay rocks and grayish-green siltstones.

4. Analytical methods

4.1. Mineralogical analyses

The detrital minerals in polished thin sections were identified, counted, and marked under an optical microscope. Powder samples were analyzed by X-ray diffraction (XRD; Empyream, PANalytical) coupled with a PIXcel3D area detector at the State Key Laboratory of Ore Deposit Geology (SKLODG), Institute of Geochemistry, Chinese Academy of Science (IGCAS). The apparatus equipped with a Dmax/2200 model diffractometer, which included the instrument standard Cu Kα target. The experiments were conducted under standard conditions at 40 kV and 20 mA, and the samples were scanned over a range of 2–60° (2θ) at a speed of 10°/min, with a step length of 0.03° (2θ). The mineral compositions of the samples were semi-quantitatively calculated using the RIR-value methods (Camden and Robert, 1988).

The morphology of minerals was observed by scanning electron microscope (SEM; JSM-7800F, JEOL) coupled with a cathodoluminescence spectrometer (MonoCL4, Gatan) at the same laboratory. Both the thin sections and mounted specimens were coated with conductive carbon film before the analyses. An energy-dispersive spectrometer (EDS; TEAM Apollo XL, EDAX) system was equipped with the SEM to quickly identify the minerals. The EDS was worked with an accelerating voltage of 20 kV, beam current of 50nA, and beam diameter of ~1 μm. The representative zircon grains were separated by conventional heavy liquid and magnetic techniques, then handpicked under a binocular microscope and mounted in epoxy. Both detrital mineral backscattered electron (BSE) images and zircon cathodoluminescence (CL) images were obtained by SEM analyses.

4.2. Major and trace elements

The whole-rock major elements were determined with wavelength X-ray fluorescence (XRF; ARL PERFORM'X 4200, Thermo Fisher) at the SKLODG, IGCAS. The samples were powered in an agate ring mill to <200 mesh, ~3 g of sample were weighed, and a composite flux of lithium borate was added to a platinum crucible before mixing. Then heated at 1150 °C until they melted to liquid, and the pelleted samples were analyzed by XRF spectrometer after cooling. The UniQuant software was used for matrix correction and calibration of data.

Powder samples of ~50 mg were weighed and digested in high-pressure Teflon bombs by using concentrated HF and HNO_3 mixture for 48 h at 190 °C. Then, the dried residues of sample solutions were dissolved in 2% HNO_3 for ICP-MS measurement. The trace elements were determined using the ME-MS61r methods at ALS Chemex Co., Ltd., Guangzhou. Before the analysis, a quantitative Rh internal standard was added to correct inter-elements interference and instrument drift. Three standards (BHVO-2, BCR-2, and GSR-1) were analyzed together with our samples, which suggested that the relative errors were generally better than 5 % for major elements and 10 % for trace elements.

4.3. Zircon U–Pb dating and trace elements

The zircon U–Pb isotopes and trace elements were simultaneously analyzed with an Agilent 7900 ICP-MS in combination with a GeoLas 193 nm excimer ArF laser ablation system at Wuhan Sample Solution Analytical Technology, China. The detailed operating conditions for the ICP-MS instrument and laser ablation system were described by Liu et al. (2010). A laser repetition rate of 5 Hz and laser energy of 80 mJ were used, with a beam diameter of 32 μm. Zircon standard 91500 (Wiedenbeck et al., 1995) was used as an external standard for U–Pb dating, and it was analyzed twice for each group of 6 sample analyses. Zircon GJ-1 was analyzed as the unknown, and the mean $^{206}Pb/^{238}U$ age is 597.6 ± 1.8 Ma (2σ, n = 27, MSWD = 1.2), which agrees well with the recommended age (e.g., 596.2–602.7 Ma; Jackson et al., 2004). The offline raw data selection and integration of background and signals, time-drift corrections and quantitative calibrations for U–Pb dating and trace element analyses were performed with ICPMSDataCal software (Liu et al., 2010). The concordia diagrams and weighted mean ages were carried out by the Isoplot 3.0 program (Ludwig, 2003). The uncertainties on individual ages are cited as 1σ, and the weighted mean ages are given at the 95 % confidence level. The trace elements of zircons were calibrated by using references BCR-2G and BIR-1G, associated with internal standardization (Liu et al., 2008). The average analytical errors range from ca. ± 10 % for the light rare earth elements (LREE) to ca. ± 5 % for the other REEs.

4.4. Zircon Lu-Hf isotopes analyses

The in situ zircon Lu-Hf isotopic compositions were determined with a Neptune plus MC-ICP-MS coupled with a GeoLas-193 laser ablation system at the same laboratory. During the analyses, a laser repetition rate of 8 Hz and beam diameter of 44 μm were used. The analytical spots were located on top of the spots used for U–Pb dating in the CL images. Zircons 91500 and GJ-1 were used as the reference standards, and zircon Plesovice was used as an external calibration standard. The detailed operating conditions for the laser ablation system and MC-ICP-MS instrument were outlined by Hu et al. (2012). The offline selection and integration of background and signals, isobaric interference and mass fractionation corrections, and external calibrations of the Lu-Hf isotopic ratios were also conducted with ICPMSDataCal software (Liu et al., 2010). The zircon standard 91500 and GJ-1 yielded weighted mean $^{176}Hf/^{177}Hf$ ratios of 0.282292 ± 16 (2σ) and 0.282008 ± 16 (2σ), respectively. These data agree well with the reported $^{176}Hf/^{177}Hf$ ratios of 0.282306 ± 10 (2σ) for 91500 from solution analyses (Woodhead et al. 2004) and of 0.282000 ± 10 (2σ) for GJ-1 from in situ analyses (Morel et al., 2008). The decay constant that adopted for ^{176}Lu was 1.867×10^{-11} yr^{-1} (Söderlund et al., 2004) and was used in all calculations. The εHf(*t*) values were calculated relative to the chondritic reservoir with a $^{176}Hf/^{177}Hf$ ratio of 0.282772 and $^{176}Lu/^{177}Hf$ ratio of 0.0332 (Blichert-Toft and Albarède, 1997). The single-stage model ages (T_{DM1}) were calculated using the measured $^{176}Lu/^{177}Hf$ ratios relative to the depleted mantle with a present-day $^{176}Hf/^{177}Hf$ ratio of 0.28325 and $^{176}Lu/^{177}Hf$ ratio of 0.0384 (Griffin et al., 2000), and the two-stage model ages (T_{DM2}) were calculated by assuming a mean $^{176}Lu/^{177}Hf$ value of 0.015 for the average continental crust (Vervoort and Blichert-Toft, 1999). The initial $^{176}Hf/^{177}Hf$ ratios were calculated by referring to the chondritic reservoir at the time of zircon growth from the magma, and the εHf(*t*) values were calculated from the $^{206}Pb/^{238}U$ ages of the zircons.

5. Results

5.1. Mineralogical composition

The fresh basalts consist of plagioclase (58–62 %), clinopyroxene (12–19 %), chlorite (8–11 %), and magnetite (~5%), with minor quartz, titanite and ilmenite. In contrast, the weathered basalts composed of plagioclase (24–37 %), kaolinite (14–28 %), chlorite (8–15 %), and quartz (5–11 %), with minor anatase, titanite, magnetite, and hematite.

The purplish-red tuffs experienced strong argillization and mainly consist of kaolinite (46–48 %), hematite (35–41 %), and anatase (13–17 %). The mineralized clay rocks are composed of kaolinite (53–67 %), montmorillonite (10–19 %), anatase (5–12 %), and minor quartz, boehmite, hematite, along with accessory zircon, rutile, Nb-rutile, columbite, and apatite (Figs. 3e–h, 4, 5). The mudstones are mainly composed of kaolinite (83–92 %), with minor montmorillonite, anatase, and quartz. The barren silty rocks contain less kaolinite (16–25 %) and more quartz (42–64 %) than the mineralized clay rocks. The siltstones from the upper part of the sections are dominated by quartz (50–65 %) and kaolinite (16–23 %), with minor montmorillonite, anatase, and hematite.

5.2. Major elements

The bulk-rock geochemical compositions of the samples from the Zhangsigou and Chahe sections are presented in Supplementary Table 1. The basalts have high Fe_2O_3 (14–16 %), MgO (3.5–4.6 %) and TiO_2 (2.7–3.5 %) contents, low Al_2O_3 (13–14 %) and CaO (~9%) contents, along with low loss on ignition (LOI; 1.4–5.6 %) and chemical index of alteration (CIA; 38–65). The degree of chemical weathering is described by the CIA values (e.g., CIA = $Al_2O_3/(Al_2O_3 + CaO^* + Na_2O + K_2O) \times 100$, in molar proportions), where CaO* represents the CaO content in the silicates (Nesbitt and Young, 1982). These basalts are characterized by high TiO_2 contents and Ti/Y ratios (Fig. 6a, d), and they belong to high-Ti basalt ($TiO_2 > 2.5$ %; Ti/Y > 500) based on the geochemical classification (Xu et al., 2001; Xiao et al., 2004). In contrast, the argillized tuffs are characterized by higher Fe_2O_3 (26.2 %) and TiO_2 (4.4 %, on average) contents, higher LOIs (5.6–9.6 %) and CIA (80–99) values. The clastic rocks in the lower Xuanwei Formation exhibit high LOIs (7.5–21.4 %) and CIA (mostly >95) values due to the high proportion of clay minerals. The polymetallic beds have high Al_2O_3 (31.1 %) contents and Al_2O_3/TiO_2 ratios (15.32), low Fe_2O_3 (10.7 %) and TiO_2 (3.1 %, on average) contents (Fig. 6a). However, the barren samples show low Al_2O_3 (22.6 %) contents and Al_2O_3/TiO_2 ratios (6.36), and high Fe_2O_3 (21.1 %) and TiO_2 (3.7 %, on average) contents.

5.3. Trace and rare earth elements

In this study, samples with Nb ≥ 112 ppm (cutoff grade of Chinese industry standards; DZ/T 0203-2020, 2020) are defined as “mineralized samples”, while those with Nb < 112 ppm are referred to as “barren samples” (Figs. 6, 7). The mineralized samples have Nb contents range from 114 to 812 ppm (298 ppm on average), and they are also enriched

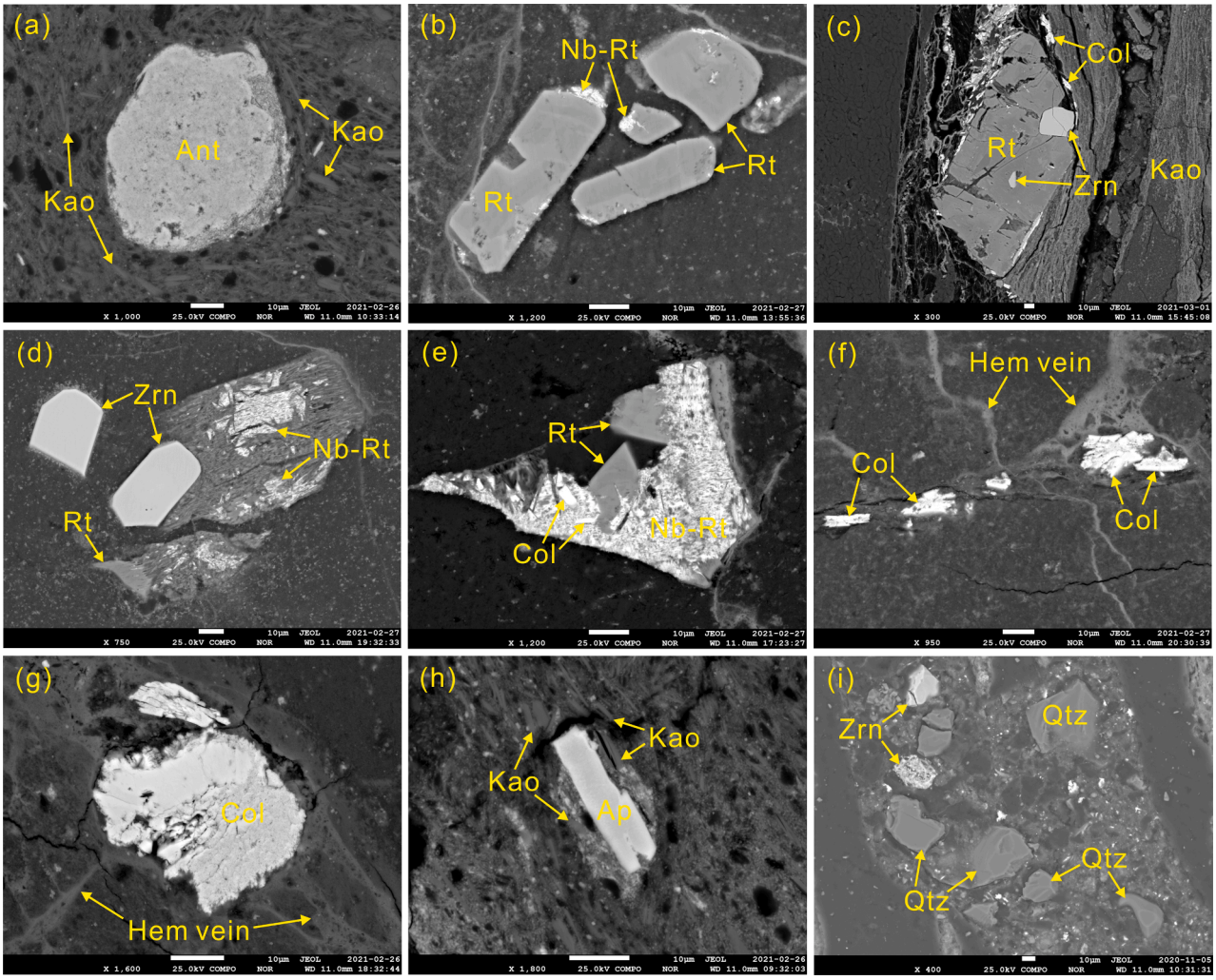

Fig. 4. Backscattered electron images of detrital minerals in the mineralized samples. (a) Anatase and kaolinite in sample CH-09H1; (b) Primary rutile replaced by Nb-rutile in sample HSZ-11H2; (c) Zircon inclusions in rutile, fine columbite and kaolinite in sample HSZ-11H2; (d) Zircon, rutile overprinted by Nb-rutile in sample HSZ-09H1; (e) Rutile enveloped by Nb-rutile and columbite in sample HSZ-11H1; (f, g) Columbite grains and hematite veins in sample HSZ-11H2; (h) Apatite and kaolinite in sample HSZ-13H2; (i) Quartz and zircon in sample CH-15H. Abbreviation: Ant: Anatase; Rt: Rutile; Col: Columbite; Zrn: Zircon; Qtz: Quartz; Ap: Apatite; Kao: Kaolinite; Hem: Hematite.

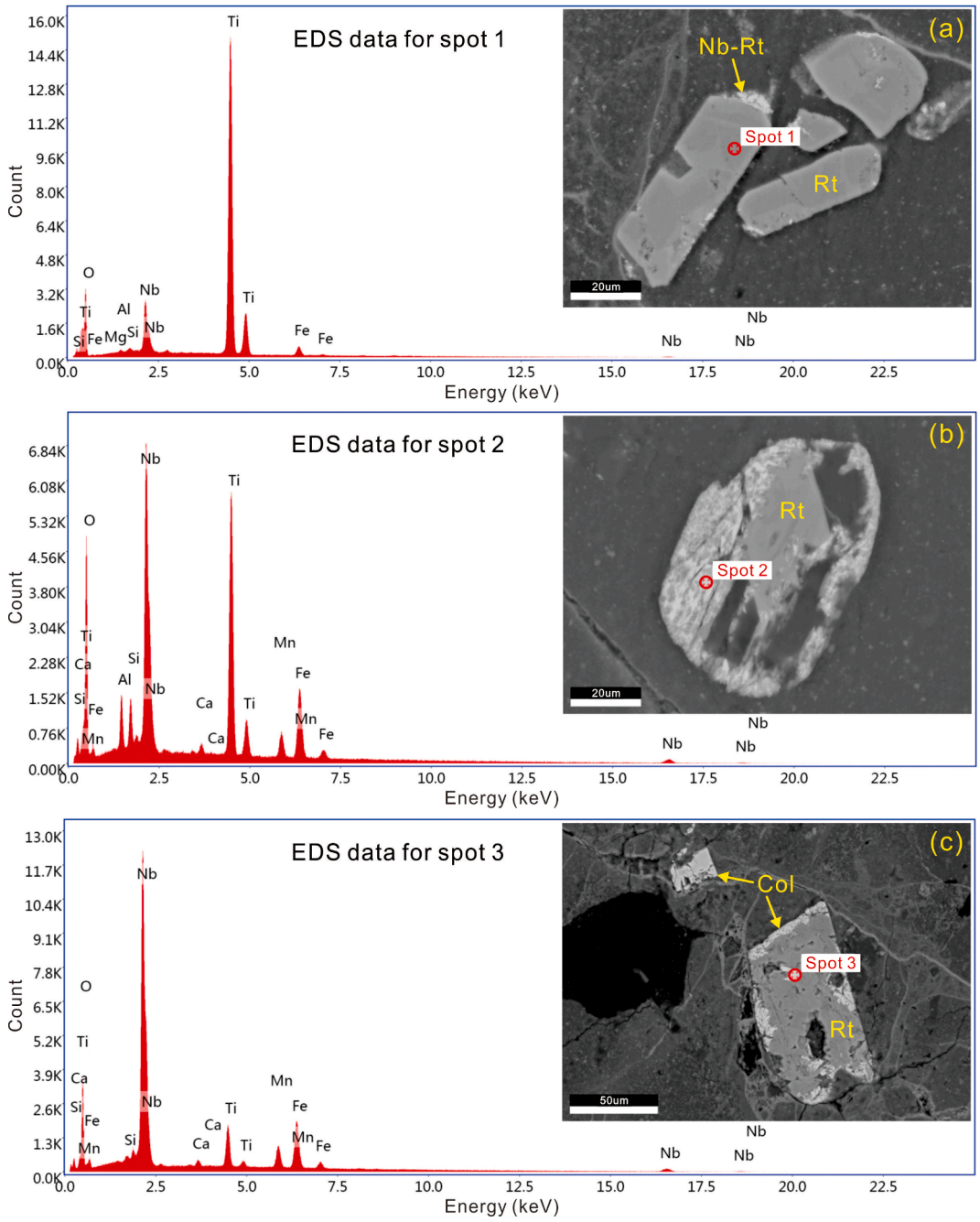

Fig. 5. Modes of occurrence of detrital rutile, Nb-rutile, and columbite in horizon HSZ-11H and EDS spectra for selected spots. (a) Primary Nb-bearing rutile (spot 1) replaced by Nb-rutile; (b) Primary rutile overprinted by Nb-rutile (spot 2); (c) Primary rutile surrounded and filled by columbite (spot 3); mineral abbreviations as in Fig. 4.

in Zr at 2231 ppm, ∑REY at 1669 ppm, and Ga at 67 ppm (on average). The barren samples contain lower Nb of 71 ppm, Zr of 517 ppm, ∑REY of 634 ppm, and Ga of 43 ppm (on average). The average Nb contents of the basalts and volcanic tuffs are 34 ppm and 41 ppm, respectively. Most mineralized samples have high Th/Sc and low Ti/Y ratios (averages of 3.16 and 267, respectively; Fig. 6b, d), but the barren samples have low Th/Sc and high Ti/Y ratios (averages of 0.44 and 560, respectively), which are similar to those of basalts and tuffs (Th/Sc < 0.35; Ti/Y > 500). The mineralized samples have high Nb/Y and Zr/TiO_2 ratios (averages of 2.32 and 0.126, respectively), whereas the barren samples have lower Nb/Y and Zr/TiO_2 ratios (averages of 0.36 and 0.016, respectively) and plot close to the basalts (Fig. 6c).

For the chondrite-normalized REE patterns (Fig. 7a, c, e, g), the high-Ti basalts and mafic tuffs exhibit a slight LREE-enriched pattern (La_N/Yb_N = 9–12) with no or slightly positive Eu anomalies. The barren samples show LREE-rich patterns and have no or weak negative Eu anomalies (Eu/Eu* on average of 0.9). The mineralized samples have LREE-rich patterns and variable La_N/Yb_N values (5–31) and are characterized by strong negative Eu anomalies (Eu/Eu* mostly in 0.3–0.7, 0.5 on average; Fig. 6d). On the primitive mantle-normalized spidergrams (Fig. 7b, d, f, h), the high-Ti basalts exhibit weak negative Sr and Rb anomalies, and their trace element patterns are relatively flat and fit well with those of ocean island basalt (OIB; Sun and McDonough, 1989). Both the tuffs and barren samples exhibit negative Rb, Sr, and Ba anomalies, with few barren samples displaying positive LREE anomalies. In contrast, the mineralized samples show strong negative Ti, Eu, Ba,

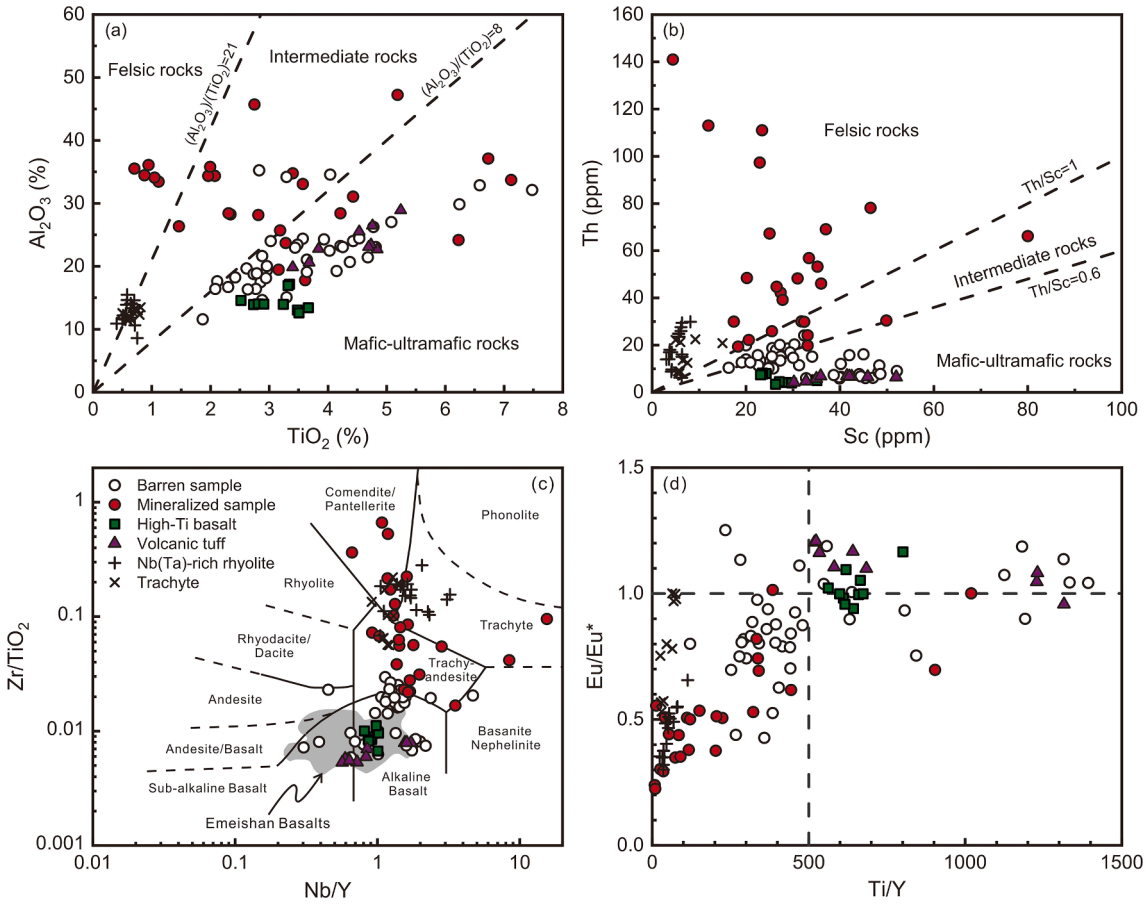

Fig. 6. (a) TiO_2 vs Al_2O_3 diagram (Hayashi et al., 1997); (b) Sc vs Th diagram (McLennan et al., 1993); (c) Nb/Y vs Zr/TiO_2 diagram (Winchester and Floyd, 1977), The zone of the Emeishan basalts (Xu et al., 2001; Xiao et al., 2004; Li et al., 2017; Liu et al., 2017); (d) Ti/Y vs Eu/Eu* diagram, Ti/Y ratio (=500) is based on the classification of the Emeishan basalts (Xu et al., 2001). Data for Nb(Ta)-rich rhyolites in the Binchuan area (Xu et al., 2010; Hei et al., 2018) and trachytes in the Panzhihua area (Shellnutt and Jahn, 2010; Xu et al., 2010) are shown for comparison.

and Sr anomalies, and significant positive HFSEs (high field strength elements) and REEs anomalies.

5.4. Zircon U–Pb ages

The detrital zircons from the polymetallic beds are clear and euhedral, with tetragonal dipyramids and oscillatory zoning in the CL images (Fig. 8). Few inherited zircons are distinguished by homogenous internal structures and core-rim structures. Most zircon grains have sub-regular, long prismatic morphologies, and well-sorted grain population. The zircons from samples CH-09H1, CH-15H, and HSZ-09H2 are relatively uniform in sizes (50–150 μm) and have length to width ratios of 1:1 to 3:1. Notably, sample HSZ-11H2 contains coarse zircon grains (200–300 μm) with length to width ratios of 1:1 to 5:1. The Th and U contents of the magmatic zircons are generally high, and the Th/U ratios are commonly >0.4, whereas the Th and U contents of the metamorphic zircons are relatively low, with Th/U ratios <0.1 (Hoskin and Schaltegger, 2003). All analyzed zircons have high Th/U ratios (0.27–1.92) and they are mostly >0.4 (Supplementary Table 2), which indicate a magmatic origin.

The U–Pb isotopic compositions of 206 zircon grains from the polymetallic beds are listed in Supplementary Table 2. Forty-two concordant analyses from sample HSZ-09H2 yield a weighted mean $^{206}Pb/^{238}U$ age of 258.7 ± 2.1 Ma, with an MSWD value of 2.2. Two grains yield concordant $^{206}Pb/^{238}U$ ages of 2482 Ma and 773 Ma, and they are older than the majority of the analyses. One grain from sample HSZ-11H2 yields a concordant $^{206}Pb/^{238}U$ age of 279 Ma, which is older than other analyses. The remaining 55 analyses are formed a tight age cluster, which yields a weighted mean $^{206}Pb/^{238}U$ age of 256.2 ± 1.5 Ma with an MSWD value of 1.1 (Fig. 9a). Furthermore, one grain from sample CH-09H1 yields a concordant $^{206}Pb/^{238}U$ age of 2219 Ma, which is significantly older than other analyses. The remaining 43 concordant ages of sample CH-09H1 yield a weighted mean $^{206}Pb/^{238}U$ age of 259.2 ± 1.8 Ma with an MSWD value of 1.4. Forty-three concordant analyses from sample CH-15H yield a weighted mean $^{206}Pb/^{238}U$ age of 258.7 ± 1.1 Ma, with an MSWD value of 1.8. The remaining four grains yield concordant $^{206}Pb/^{238}U$ ages of 593 Ma to 281 Ma, and they are older than the majority of the analyses (Fig. 9b).

5.5. Zircon trace elements

The chemical compositions of 191 zircons with concordant ages of 2482 Ma to 249 Ma are listed in Supplementary Table 3. For the chondrite-normalized REE patterns, most zircons increase sharply from La to Lu, with positive Ce anomalies and extremely negative Eu anomalies (Fig. 10a). The Eu/Eu* values of the analyzed zircons are generally <0.3, with an average of 0.2. Nevertheless, some zircons show LREE-enriched patterns with slightly positive Ce anomalies, along with high P contents (>800 ppm). Despite the intergrowth of zircon and rutile (Fig. 3g, h, 4c, d), the analyzed zircons exhibit low Ti contents (mostly <20 ppm). Based on the Ti-in-zircon thermometer (Ferry and Watson, 2007), the calculated crystallization temperatures (T_{Zr}) of the zircons are generally <800 °C, with mean T_{Zr} of 734 °C, 703 °C, 740 °C, and 732 °C for the zircon groups from samples HSZ-09H2, HSZ-11H2, CH-09H1, and CH-15H, respectively (Fig. 10b).

The zircons from the Zhangsigou section show high Nb and low Hf

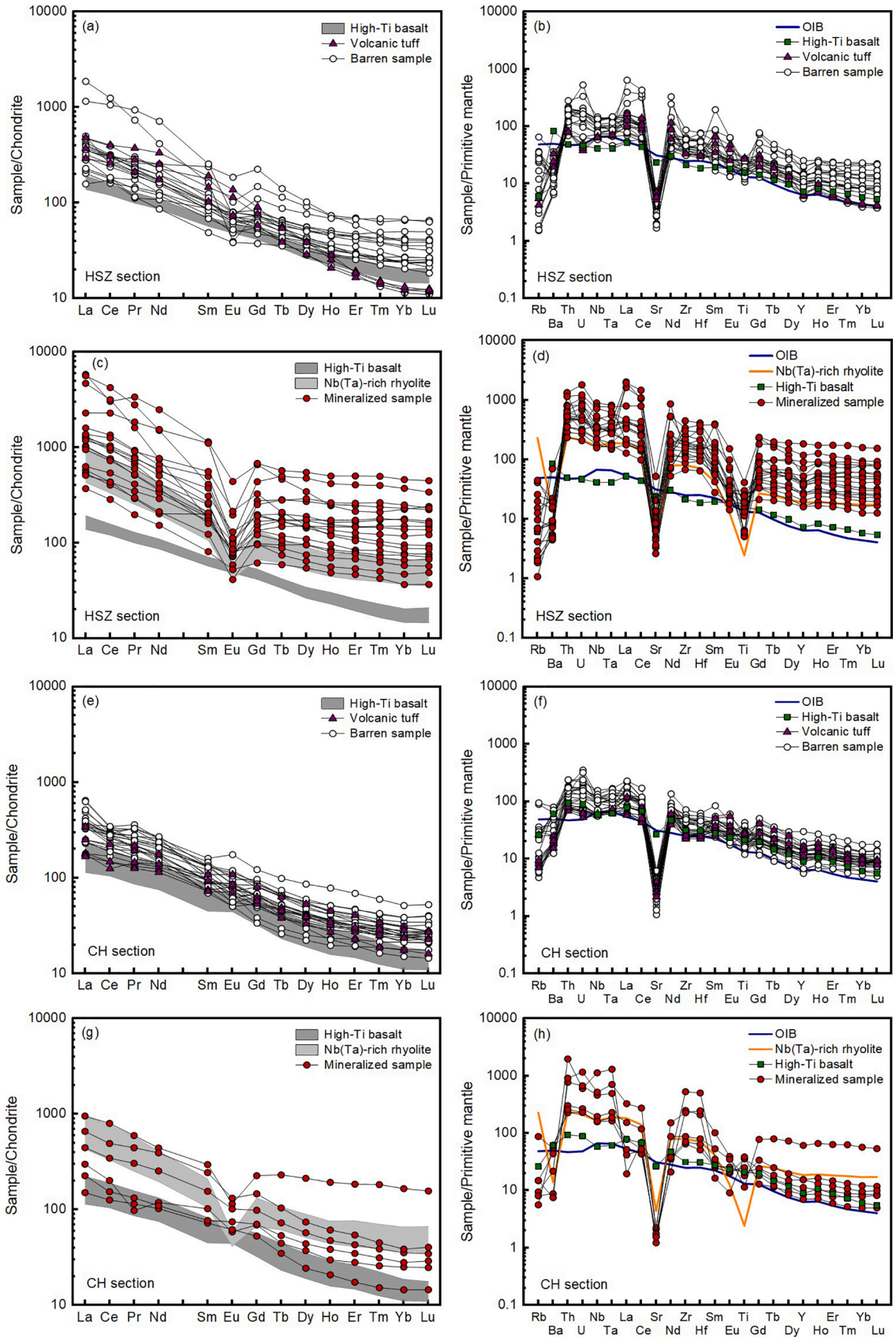

Fig. 7. Chondrite (Taylor and McLennan, 1985) normalized rare earth element (REE) patterns and primitive mantle (Sun and McDonough, 1989) normalized trace element spidergrams of samples in the Zhangsigou (a, b, c, d) and Chahe (e, f, g, h) sections. Trace elements for Nb(Ta)-rich rhyolites (Xu et al., 2010; Hei et al., 2018) and ocean island basalt (OIB; Sun and McDonough, 1989) are shown for comparison.

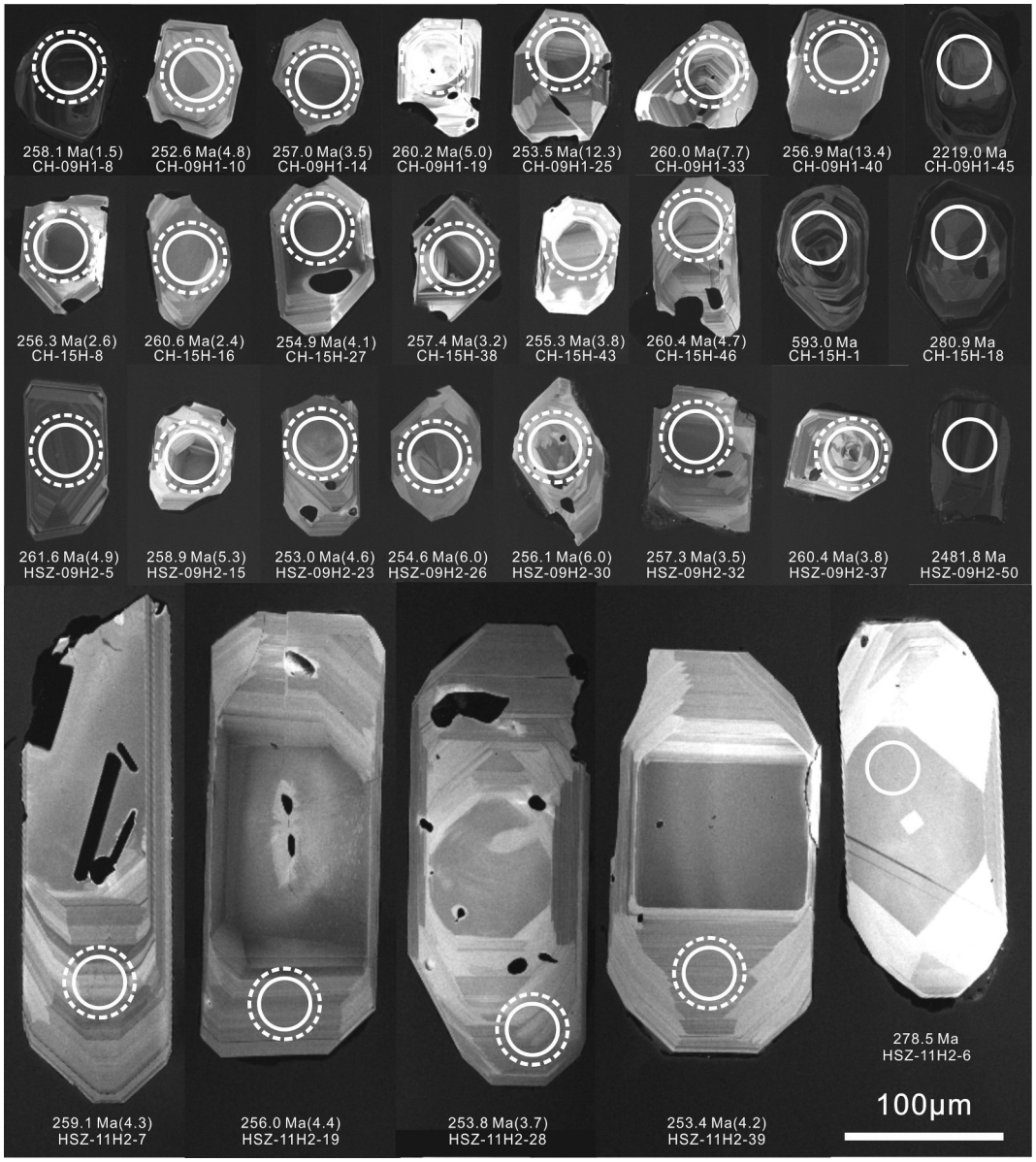

Fig. 8. Representative cathodoluminescence images of detrital zircons from the polymetallic beds. The white solid and dashed circles denoted each spot of the U−Pb and Lu-Hf isotope analyses, respectively. The εHf(*t*) values correspond to the U−Pb ages are shown in the brackets. The coarse zircons (200–300 μm) with rutile and apatite inclusions are from sample HSZ-11H2.

contents (averages of 13.4 ppm and 7706 ppm, respectively), whereas the zircons from the Chahe section show lower Nb and higher Hf contents (averages of 10.1 ppm and 8447 ppm, respectively). The zircon grains with concordant ages are plotted on the Nb/Yb vs U/Yb and Th/Nb vs Hf/Th diagrams, respectively (Fig. 11). The Late Permian (~260 Ma) zircons from the Zhangsigou section exhibit low Th/Nb and U/Yb ratios (averages of 7.25 and 0.41, respectively). In contrast, the ~260 Ma zircons from the Chahe section show higher Th/Nb and U/Yb ratios (averages of 42.56 and 0.65, respectively). Furthermore, the older zircons with concordant U−Pb age >280 Ma are characterized by high Th/Nb and U/Yb ratios (averages of 100.41 and 1.08, respectively).

5.6. Zircon Lu-Hf isotopic compositions

The Lu-Hf isotopic compositions for 118 zircons with U−Pb ages in the range of 270–249 Ma are listed in Supplementary Table 4. Twenty-seven analyses from sample HSZ-09H2 exhibit high initial $^{176}Hf/^{177}Hf$ ratios of 0.282403–0.282788, which correspond to εHf(*t*) values of −7.3 to +6.0. Thirty-seven zircons from sample HSZ-11H2 yield relatively low $^{176}Hf/^{177}Hf$ ratios of 0.282715–0.282752, with homogeneous εHf(*t*) values of +3.5 to +4.9. Additionally, 27 zircon grains from sample CH-09H1 show high initial $^{176}Hf/^{177}Hf$ ratios of 0.282500–0.283001, with εHf(*t*) values of −4.1 to +13.4. Twenty-seven analyses from sample CH-15H exhibit relatively low $^{176}Hf/^{177}Hf$ ratios of 0.282327–0.282950, with εHf(*t*) values varying from −10.1 to +11.9 (Fig. 12a). The zircon εHf(*t*) values from the polymetallic beds mainly range from +2.0 to +6.0, which correspond to Hf model ages (T_{DM1}) of 820–660 Ma. Five analyses from the Chahe section exhibit high positive εHf(*t*) values (+11.2 – +13.4), and the remaining analyses show two distinct groups for the zircon εHf(*t*) values and Hf model ages. The first group shows negative εHf(*t*) values of −4.1 to −0.5, which correspond to T_{DM1} of 1067–956 Ma and T_{DM2} of 1539–1321 Ma. Another group exhibits more negative εHf(*t*) values of −10.1 to −7.3, which correspond to T_{DM1} of 1306–1195 Ma and T_{DM2} of 1921–1747 Ma.

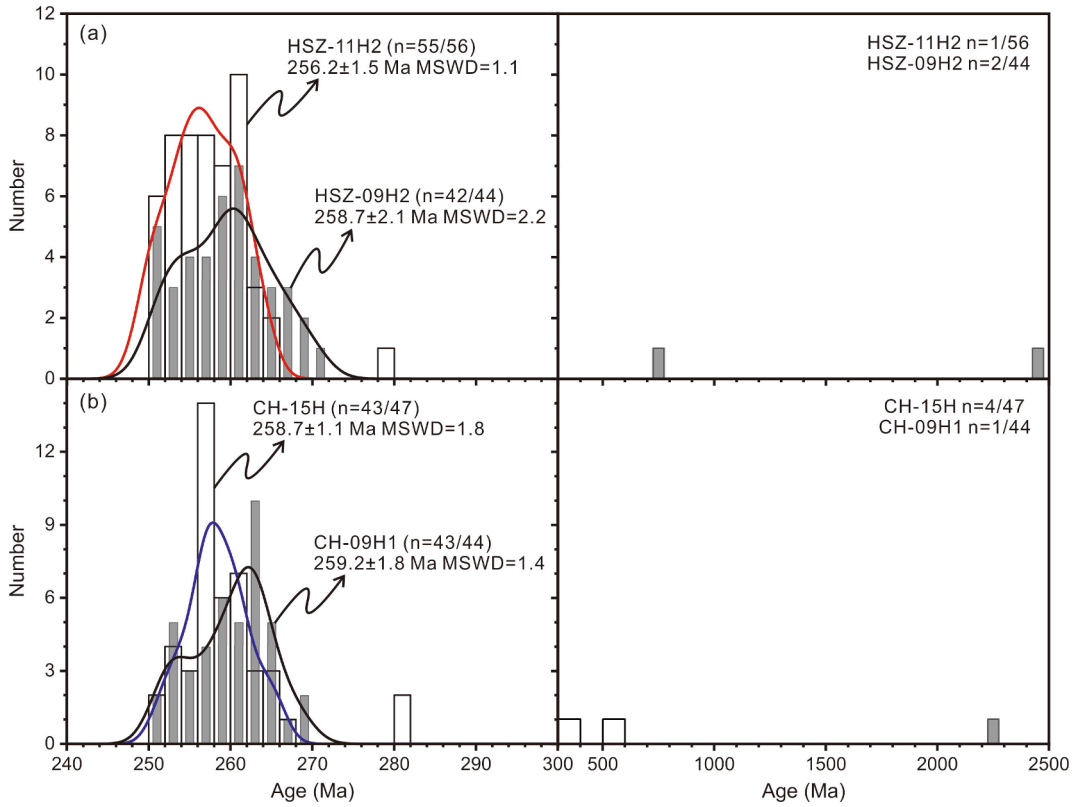

Fig. 9. Date distribution and probability density diagram for the detrital zircons with concordant U−Pb ages from mineralized samples in the Zhangsigou section (a) and the Chahe section (b). "HSZ-09H2 (n = 42/44)" denotes the sample name and number of analyses for calculating the weighted mean age and for plotting the probability density; "HSZ-09H2 n = 2/44" denotes the number of analyses with concordant U−Pb ages older than the majority of analyses.

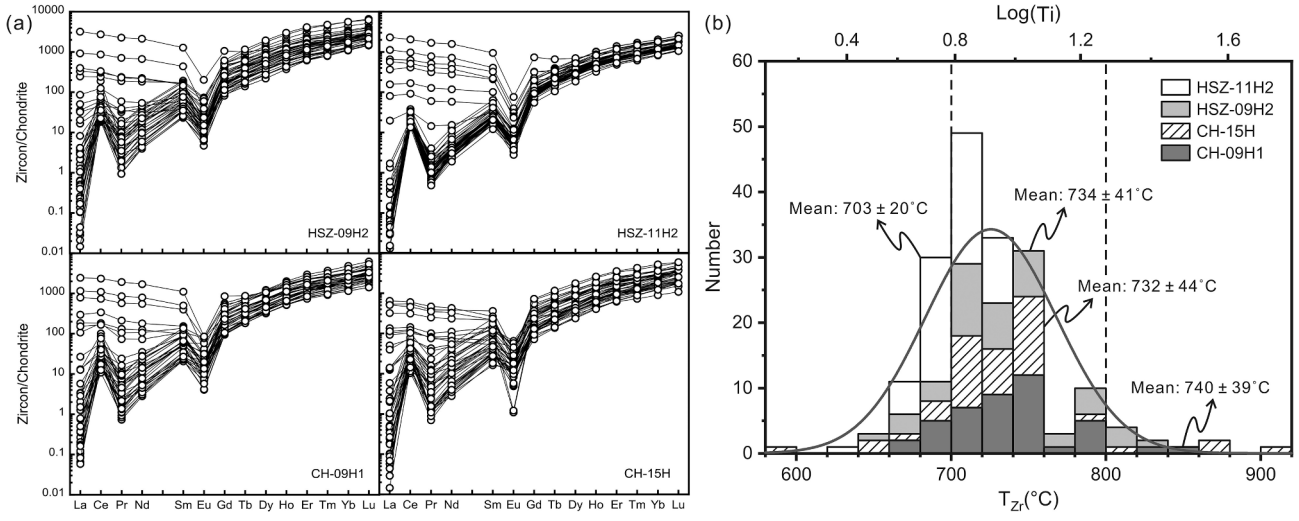

Fig. 10. (a) Chondrite (Taylor and McLennan, 1985) normalized REE patterns for zircons from mineralized samples and (b) Distribution of Ti contents (Log Ti ppm) and crystallization temperatures (T_{Zr}) of zircons. The Ti-in-zircon thermometer is from Ferry and Watson (2007); the calculated values in histogram represent mean T_{Zr} with 2SD for each sample.

6. Discussion

6.1. Provenance of the lower Xuanwei Formation

The polymetallic beds are characterized by high Al_2O_3 contents, low Fe_2O_3 and TiO_2 contents, whereas the barren samples exhibit high Fe_2O_3 and TiO_2 contents, and low Al_2O_3 contents, which are akin to those of the high-Ti basalts and mafic tuffs. The Al_2O_3/TiO_2 and Th/Sc ratios remain nearly constant during supergene weathering and chemical alteration and have been used as indicators of the provenance of clastic rocks (McLennan et al., 1993; Hayashi et al., 1997). On the TiO_2 vs Al_2O_3 and Sc vs Th diagrams (Fig. 6a, b), the mineralized samples plot mainly within the area of intermediate to felsic rocks (Al_2O_3/TiO_2 >8; Th/Sc >0.6), and show affinities to the Nb(Ta)-rich rhyolites (Xu et al., 2010; Hei et al., 2018) and trachytes (Shellnutt and Jahn, 2010; Xu et al., 2010) that are located at the top of the Emeishan lavas. In contrast,

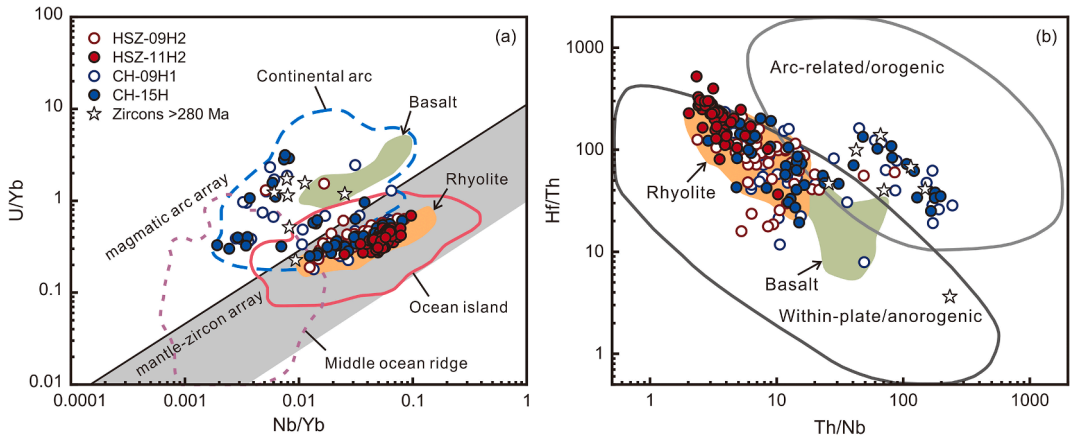

Fig. 11. (a) Nb/Yb vs U/Yb (Grimes et al., 2015) and (b) Th/Nb vs Hf/Th (Yang et al., 2012) diagrams for zircons from the polymetallic beds. The zircon data for the rhyolites and basalts in the Shangcang section (Huang et al., 2022) are shown for comparison.

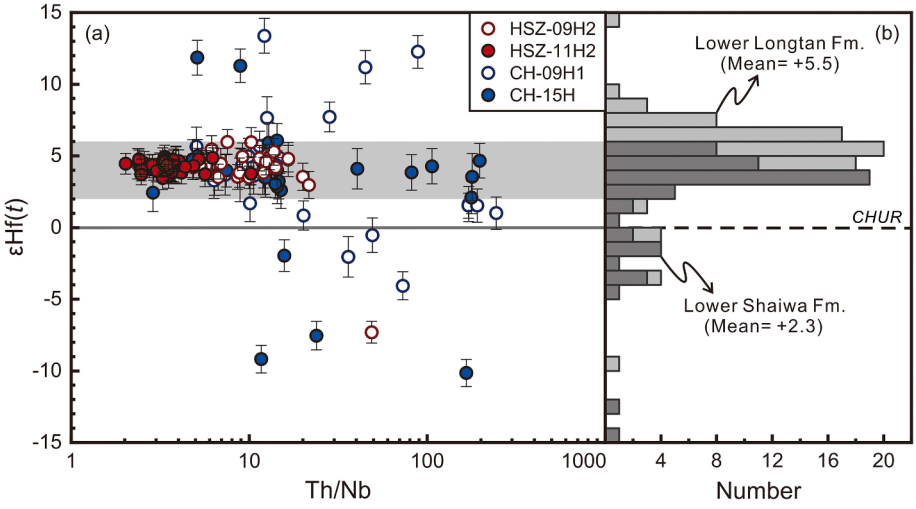

Fig. 12. (a) Zircon Th/Nb vs εHf(*t*) plot for the mineralized samples in the lower Xuanwei Formation; (b) Distribution of zircon εHf(*t*) values in the lower Shaiwa Formation (Yang et al., 2015) and lower Longtan Formation (Deng et al., 2020); The mean zircon εHf(*t*) values are calculated from all analyzed samples.

the barren samples mostly fall within the area of mafic-ultramafic rocks (Al_2O_3/TiO_2 <8; Th/Sc <0.6), which are similar to the underlying basalts and tuffs. Furthermore, on the Nb/Y vs Zr/TiO_2 diagram (Winchester and Floyd, 1977), the basalts and tuffs plot within the zone of the Emeishan basalts (Fig. 6c). The mineralized samples are distributed in the trachy-andesite, trachyte, and pantellerite area on this diagram, which is consistent with the Nb(Ta)-rich rhyolites and trachytes from the Emeishan LIP inner zone. But the barren samples mainly plot within the area of basaltic rocks and close to the zone of the Emeishan basalts. In addition, the mineralized samples exhibit strong negative Eu anomalies and low Ti/Y ratios, which are similar to those of silicic extrusive rocks. But the barren samples are comparable to basalts and tuffs with weak negative or no Eu anomalies and high Ti/Y ratios (Fig. 6d). These characteristics suggest that the clastic sediments of the lower Xuanwei Formation are derived from both the mafic and felsic parts of the Emeishan volcanic rocks.

For the chondrite-normalized REE distribution patterns and primitive mantle-normalized spidergrams (Fig. 7), most of the mineralized samples show similar trace element patterns that are parallel to those of the Nb(Ta)-rich rhyolites, whereas the trace element patterns of the barren samples are similar to those of the underlying basalts and tuffs. Overall, the mineralized samples from the lower Xuanwei Formation show geochemical affinities with the felsic eruptive rocks of the Emeishan LIP, which were proposed to have generated by the fractional crystallization of OIB-like mantle magmas (Shellnutt and Jahn, 2010; Xu et al., 2010; Cheng et al., 2017; Hei et al., 2018; Huang et al., 2022). On the other hand, the mineralized samples exhibit strong negative Ti, Eu, Ba, and Sr anomalies, along with positive HFSEs and REEs anomalies on the spidergrams (Fig. 7d, h). These trace elemental anomalies imply that the silicic source rocks have experienced fractionation of a gabbroic melt, which produced layered mafic intrusions and massive Fe-Ti oxide deposits (Shellnutt and Jahn, 2010; Xu et al., 2010). The provenance features of the lower Xuanwei Formation are consistent with the unroofing model of the Emeishan LIP (He et al., 2007). However, our data indicate that the barren samples, including tuffaceous and ferriferous clays at the bottom of the Xuanwei Formation exhibit more affinities to the altered basalts and tuffs in terms of geochemical and mineralogical compositions.

More importantly, the polymetallic beds in this study are characterized by detrital minerals, including zircon, quartz, apatite, rutile, Nb-rutile, and columbite (Figs. 3e–h, 4, 5). These minerals are common in alkaline silicic rocks but are rare in the underlying high-Ti basalts and mafic tuffs. Such mineralogical compositions are similar to the detrital mineral assemblages (e.g., high-temperature quartz, zircon, micas, albite, rutile, and monazite) in the polymetallic enrichments of the lower Longtan Formation in western Guizhou (Liu et al., 2019; Shen et al., 2021). These mineralogical characteristics indicate that the Nb-Zr-REE-Ga-enriched beds in western Guizhou are mainly derived from distal

silicic rocks, which served as a terrigenous source.

The detrital zircons of the mineralized samples yield mean $^{206}Pb/^{238}U$ ages of 259.2 Ma to 256.2 Ma (Fig. 9). These ages are consistent with the temporal range of 261–255.6 Ma for the Binchuan rhyolites (Hei et al., 2018; Huang et al., 2022), and are synchronous with the silicic eruptive range (ca. 260–257.1 Ma) of the Emeishan volcanism (Huang et al., 2018; Shellnutt et al., 2020; Zhong et al., 2020). Additionally, the mineralized samples in the Zhangsigou section have younger zircon U–Pb ages than those in the Chahe section (Fig. 9). These results, together with the zircon ages (ca. 257 Ma) from the lowermost Xuanwei sediments (He et al., 2007), also indicate that these clastic sediments were derived from the erosional unroofing of the Emeishan silicic rocks. Whole-rock geochemistry and zircon geochronology of the Late Permian strata in the basin of eastern Emeishan LIP show a reverse succession in comparison to the central Emeishan volcanic sequence (Fig. 13). Collectively, our data suggest that the polymetallic beds in the lower Xuanwei Formation were dominantly eroded from the silicic extrusive rocks at the top of the Emeishan lavas, whereas the barren samples were likely incorporated mafic compositions.

6.2. Sedimentary records from alkaline magmatism

In this study, the minor mineralized samples exhibit higher Th/Sc ratios, Zr/TiO_2 ratios, and more negative Eu anomalies (Fig. 6) than those of the Binchuan rhyolites and Panzhihua trachytes (Shellnutt and Jahn, 2010; Xu et al., 2010; Hei et al., 2018). Meanwhile, these samples show higher La_N/Yb_N ratios, more positive HFSEs and REEs anomalies than those of the Nb(Ta)-rich rhyolites in trace element patterns (Fig. 7d, h). In comparison to the remnant rhyolites, these samples may record a more evolved magma during the late-stage Emeishan volcanism. In addition, the mineralized beds in the Zhangsigou section are characterized by niobium minerals of Nb-rutile and columbite (Figs. 4b–g, 5). The assemblage of niobian rutile and columbite-(Fe) are generally crystallized from evolved alkaline magma or magmatic hydrothermal system (Černý et al., 1989; Meinhold, 2010). The detrital Nb-rutile and columbite were also found in the correlative sediments in eastern Yunnan coalfield, which are derived from the Emeishan alkaline volcanism (Dai et al, 2016a; Wang et al., 2022). The primary rutile was replaced and overprinted by Nb-rutile and columbite with intensive Nb-replacement (Figs. 4b–e, 5), which are likely to generate from hydrothermal metasomatism during waning alkaline magmatism. Thus, the eroded volcanic rocks may include minor alkaline rocks that have been superimposed by magmatic hydrothermal activity.

The zircons from the mineralized beds are rich in apatite and rutile inclusions, with minor grains yield LREE-rich patterns, which are owing to the occurrence of REE-phosphate inclusions (Fig. 10a). These zircons exhibit strong negative Eu anomalies, and the average Eu/Eu* values decrease from 0.2 for the older sample (CH-09H1) to 0.1 for the younger sample (HSZ-11H2), which suggests that an evolved magma experienced significant plagioclase fractionation (Belousova et al., 2002; Hoskin and Schaltegger, 2003). Moreover, the zircons are associated with rutile, Nb-rutile, and columbite, with fine zircons crystallized

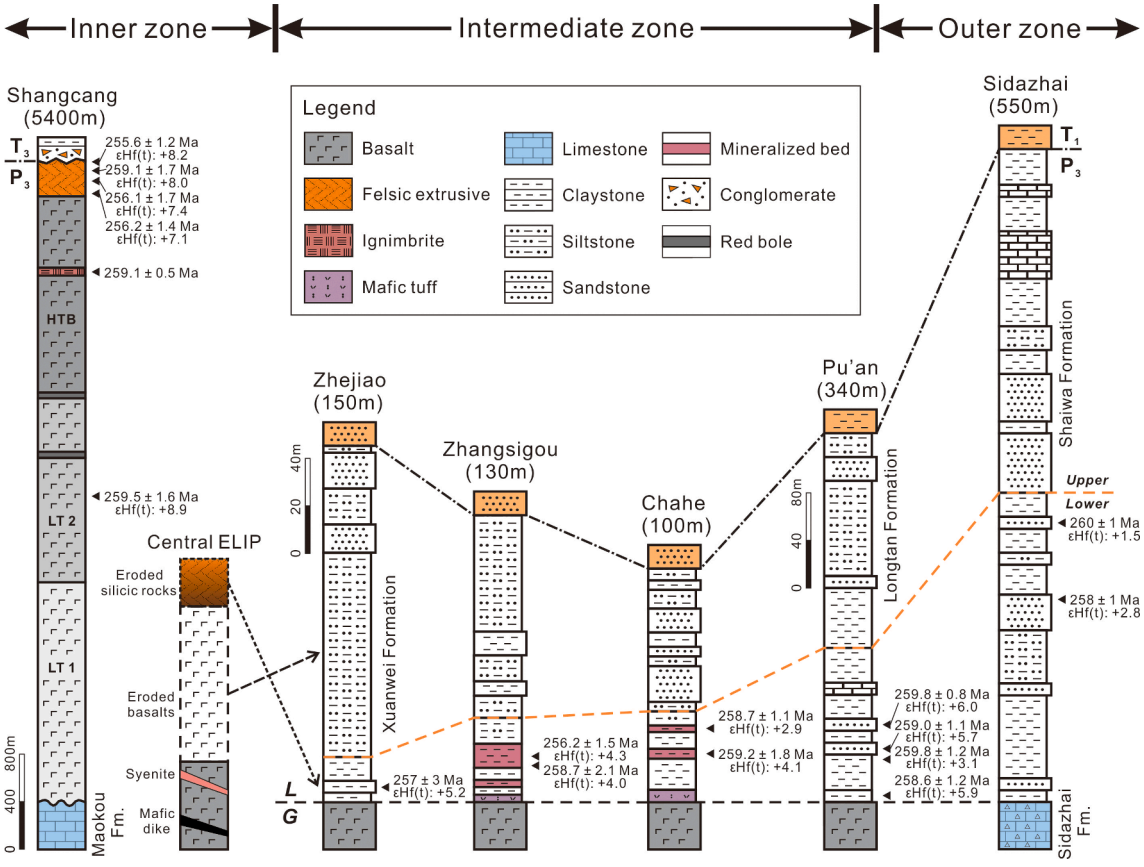

Fig. 13. Chemostratigraphic correlation of the Emeishan volcanic sequences and the sedimentary sections in the eastern Emeishan LIP. The locations of sections are shown in Fig. 1. The Shangcang section and zircon data are from Huang et al. (2022), the ID-TIMS zircon age of ignimbrite is from Zhong et al. (2014); The Zhejiao section is after He et al. (2007), and zircon data are from Xu et al. (2008); The Pu'an section and zircon data are from Deng et al. (2020); The Sidazhai section and zircon data are from Yang et al. (2015). The zircon U–Pb ages and corresponding εHf(*t*) values are denoted near the sampling horizons. Black and orange dashed lines represent the Guadalupian-Lopingian boundary and the lower–upper boundary of Upper Permian strata, respectively. The eroded volcanic sequence in central Emeishan LIP is modified after He et al. (2007). The sedimentary sequence of the Late Permian formations is the reverse succession of the Emeishan volcanic lavas in geochemical and chronological characteristics.

within the rutile grains (Figs. 3e, g, 4c, d). According to this mineral assemblage, the calculated T_{Zr} of analyzed zircons are mostly distributed in 660 °C to 800 °C (Fig. 10b). These values are consistent with the temperature range for the magmatic evolution of the Emeishan felsic rocks, as demonstrated by MELTS modeling (Shellnutt and Jahn, 2010), and are much lower than the temperatures (generally >950 °C) of basaltic magmas (Xu et al., 2010). Furthermore, the average T_{Zr} decreasing from 740 °C for older sample (CH-09H1) to 703 °C for younger sample (HSZ-11H2). The temporal variations of Eu/Eu* value and T_{Zr} of zircons suggest that the source magma experienced prolonged fractionation in a cooling trend.

On the other hand, zircon U−Pb dating of the polymetallic beds yields a temporal range of 259.2–256.2 Ma, which correspond to mean $\varepsilon Hf(t)$ values of +2.9 − +4.3 (Fig. 13). These results suggest a period of ~3 m.y. for the eroded silicic rocks, and the waning Emeishan volcanism may have lasted to the middle Wuchiapingian. Zircon U−Pb ages of the polymetallic beds are consistent with the zircon ID-TIMS ages of the alkaline volcanic ashes of the Emeishan LIP (ca. 260.8–257.3 Ma; Mundil et al., 2004; Shen et al., 2011; Zhong et al., 2020), but they are younger than the temporal range of mafic volcanisms (ca. 263–259.1 Ma; Zhong et al., 2014, 2020; Yang et al., 2018; Huang et al., 2022). Furthermore, the zircons from the younger samples are comparable to the zircons from the Nb(Ta)-mineralized syenites in the Panxi area (the Panzhihua to Xichang area in southern Sichuan Province; Fig. 1), which yield U−Pb ages of 257.8–256.7 Ma, corresponding to mean $\varepsilon Hf(t)$ values of +3.8 to +5.4 (Wang et al., 2013). These syenitic dikes are intruded into the layered gabbro and are temporally consistent with the erupted silicic rocks. Different from the polymetallic beds, the sporadic syenites are characterized by various Nb-bearing minerals, including pyrochlore, fergusonite, and titanite, which were crystallized in the magmatic-hydrothermal stage (Wang et al., 2013, 2015). The comparison of zircon U−Pb ages and Hf isotopes indicates that both the eroded source rocks, Nb(Ta)-rich rhyolites, and Nb(Ta)-mineralized syenites are the products of waning Emeishan alkaline volcanism. The eroded silicic rocks may represent the erupted equivalent of the coeval syenitic dikes, and they were generated by protracted alkaline magmatism and were enriched in rare metals.

The Nb-Ta mineralized syenitic dikes formed from a highly evolved magma and their ore-forming hydrothermal became gradually enriched in F, Ca, Nb, Ta, Zr, Hf, REE, Y, Th, and Pb (Wang et al., 2015; Zeng and Liu, 2022). The Nb(Ta) were decomposed from Nb(Ta)-fluorine complexes due to intensive albitization in the late-stage magmatic hydrothermal and finally entered into pyrochlore (Wang et al., 2015). The peralkaline granitic plutons were derived by fractional crystallization of basaltic magmas, and eventually erupted onto the surface and produced Nb-Zr-rich trachytes. The silicic residual magma likely formed near the top of the magma chamber and enriched the incompatible elements such as REEs, Nb, Ta, Zr, Hf, Th and U (Shellnutt and Jahn, 2010; Xu et al., 2010). Similarly, the Nb-Ta-rich rhyolites (also rich in Zr, Hf, Ga, REE, and Y) were generated from the alkaline silicic magmas, which formed by the fractionation of abundant mafic-ultramafic complexes and Fe-Ti oxide deposits of high-Ti basaltic magmas, and coupled with minor crustal assimilation (Xu et al., 2010; Hei et al., 2018). Therefore, the enrichment of incompatible rare metals in waning-stage alkaline magmatism of the Emeishan ELIP may be responsible for the mineralization of Late Permian polymetallic beds in southwestern China.

6.3. New insights into the origin of polymetallic beds

Previous study proposed that the polymetallic enrichments in western Guizhou were formed in the weathering crust of the underlying basalts (Huang, 1997; Yang et al., 2008) or deposited from the weathered materials of the Emeishan basalts (Zhou et al., 2013; Zhang et al., 2016). In this study, the polymetallic beds are composed of thick-bedded clay rocks and thin mudstone layers, which are deposited over the pre-erupted basalts and are separated by tuffaceous and ferriferous clays (Figs. 2, 3a, b). The sedimentary sequence implies that these beds were formed in the volcanic depressions that shaped by the uplift of mantle plume and the eruption of flood basalts. In addition, the mineralogical and geochemical compositions suggest that these beds are sourced from silicic rocks rather than basaltic rocks (Figs. 4–7). The coal seams in the sampling sections are 0.1–0.3 m in thickness and are sandwiched by hard clay rocks, which are deposited as the roof and floor of the coal seams (Fig. 3a, c). Unlike these clay rocks, the mineralized tonsteins in eastern Yunnan coalfield were formed within coal seams (Zhou et al., 2000; Dai et al., 2010; Zhao et al., 2016). The thick-bedded clay rocks in this area were deposited in the sedimentary facies of alluvial plain, fan delta, swamp, and lake, and they were dominantly fed by terrigenous clasts from the Chuandian old land (Zhang et al., 2010; Zhou et al., 2013; Wang et al., 2020). In contrast, the intra-coal tonsteins from eastern Yunnan were formed in the proximal peat swamps of eruption center, which were proposed to deposit from airborne volcanic ashes (Zhou et al., 1982; Zhao et al., 2016).

Based on the preliminary analyses, we inferred that the Nb and Zr are mainly hosted in the heavy minerals (Nb: rutile, ilmenorutile, columbite, anatase; Zr: zircon), whereas the REY and Ga are likely to occur as finely dispersed minerals (e.g., florencite, diaspore) and adsorbed ions within the clay minerals. In the polymetallic beds, most of the detrital rutile, quartz, zircon, and columbite are subangular to subrounded (Figs. 3e−h, 4), with well-sorted grain populations (in sizes of 50–150 μm). Incidentally, the zircon grains from horizon HSZ-11H are ranging from 200 μm to 300 μm (Fig. 8). Furthermore, some rutile, zircon, columbite, and apatite are in columnar shape, and they are oriented and paralleled to the bedding of clay layers (Fig. 3g, h, 4b, c, f, h). These features reflect that the terrigenous clasts are likely to transport in fluvial way. Similarly, the rounded quartz, micas, zircon, albite, and rutile in the polymetallic beds of the Longtan Formation are proposed to erode from a distal silicic source (Liu et al., 2019; Shen et al., 2021). The polymetallic beds in western Guizhou and Nb-Zr-REE-Ga-rich tonsteins in eastern Yunnan are analogous in geochemical and mineralogical compositions, which suggest that they are comagmatic, and are both sourced from the Emeishan alkaline volcanisms.

The widespread nature of the Nb-Zr-REE-Ga enrichment in southwestern China indicates the presence of voluminous amounts of alkaline rocks in the uppermost Emeishan lavas. Based on the clastic modal and geochemical data from the Shaiwa and Longtan formations, the eroded silicic rocks were estimated to have a volume over 3×10^4 km^3, which contributed ~25 % by weight ratio to the Late Permian detrital sediments in the northern Youjiang Basin (Yang et al., 2015, 2018). Furthermore, Deng et al. (2020) proposed that the clastic rocks of the lower Longtan Formation in western Guizhou were dominantly derived from late-stage Emeishan silicic volcanism. On the other hand, the silicic rocks at the top of the Emeishan lavas are characterized by high HFSE and REE contents. For example, the rhyolites from the central Emeishan LIP show high concentrations of Nb (100–160 ppm), Zr (700–1200 ppm), and ∑REE (400–1100 ppm; Xu et al., 2010; Cheng et al., 2017; Hei et al., 2018), and the trachytes from the Panzhihua area are enriched in Nb (80–170 ppm), Zr (500–1300 ppm), and ∑REE (400–1000 ppm; Shellnutt and Jahn, 2010; Xu et al., 2010). Therefore, the alkaline rocks and tuffs at the top of the Emeishan volcanic sequence show great potential in the Nb-Zr-REE mineralization. These rocks have considerable volumes and rare metals to serve as a persistent source for the enrichments in the lower Xuanwei Formation and synchronous strata.

Taken together, the mineralization of polymetallic beds is associated with the waning Emeishan alkaline magmatism, and they are cogenetic with the mineralized tonsteins in eastern Yunnan Province (Zhou et al., 2000; Dai et al., 2010; Zhao et al., 2016), as well as alkaline volcanic ashes at the periphery of the Emeishan LIP (He et al., 2010; Huang et al., 2018; Zhong et al., 2020). The eroded source rocks were concentrated by the extensive fractionation of alkaline magma, then erupted, and experienced strong tropical weathering. The weathered materials (with residual Nb, Ta, Zr, Hf, Y, Ga, and REEs) were mainly transported by

subaerial drainage and deposited in swamps or lakes, which were followed by further enrichment of diagenetic processes (Fig. 14). Similarly, the Nb(Ta)-Zr(Hf)-REY-Ga enriched coals and host rocks in the south of Kuznetsk Basin, Russia and the Daqingshan Coalfield, northern China are related to the input of alkaline volcaniclastics of felsic composition during peat accumulation (Arbuzov et al., 2019; Zhao et al., 2019). The Nb-Zr-REE-Ge-U mineralization is altered from the alkaline tuffs and mixed hydrothermal overprinting in the coal basins of South Primorye, Russia (Seredin and Finkelman, 2008; Dai et al., 2016a). Unlike the mineralization in coal-bearing strata, the Pitinga Nb-Zr-REY-Sn-Th deposit in the Amazonas State, northern Brazil is resulted from intensive weathering and lateritization of alkaline granite, and the leaching of alkalis and allitization led to relative enrichment of rare metals in the saprolitic and lateritic horizons (Horbe and Costa, 1999; Alves et al., 2018). In comparison, Lazareva et al. (2015) proposed that the lacustrine sediments of Tomtor Nb-REE-Y-Sc deposit in the northern Sakha Republic, Russia are weathered from REE-phosphates enriched carbonatites and most ore minerals are precipitated from hydrothermal fluids. In this study, the metallogenic model sheds new light on the distribution of the Emeishan volcanism-related Nb-Zr-REE-Ga mineralization in southwestern China. Such a polymetallic enrichment is likely to develop in the lower Shaiwa and Wujiaping formations in the basin of eastern Emeishan LIP, and may extend to the synchronous strata and volcanic ashes located outside the Emeishan LIP.

6.4. *Implications for the late-stage Emeishan volcanism*

The Late Permian zircons from the polymetallic beds yield εHf(*t*) values in the range of −10.1 – +13.4 (on averages of +2.9 – +4.3; Fig. 12a). In comparison, the alkaline rhyolites in the Emeishan LIP inner zone yield zircon εHf(t) values of −11.9 – +12.9 (Usuki et al., 2015; Hei et al., 2018; Huang et al., 2022). But the zircons from the Emeishan basalts yield mean U−Pb age of 259.5 Ma, which correspond to mean εHf(*t*) value +8.9 (Huang et al., 2022). The chronological and Hf isotopic features of the detrital zircons in the polymetallic beds are consistent with those of the zircons obtained from the remnant rhyolites. Furthermore, the extremely negative Eu anomalies of the zircons (Fig. 10a), along with the strong negative Ti, Eu, and Ba anomalies of the mineralized samples (Fig. 7d, h), corresponding to the fractional crystallization dominated processes for the generation of extrusive silicic rocks in the central Emeishan LIP (Shellnutt and Jahn, 2010; Xu et al., 2010; Cheng et al., 2017; Hei et al., 2018; Huang et al., 2022).

The Nb/Yb vs U/Yb and Th/Nb vs Hf/Th diagrams (Yang et al., 2012; Grimes et al., 2015) have been successfully used to trace the tectonomagmatic provenance for zircons from Upper Permian strata and volcanic ashes in southwestern China (Yang et al., 2015; Huang et al., 2018; Deng et al., 2020; Zhong et al., 2020). In these diagrams, most Late Permian zircons are located in the ocean island area and the within-plate/anorogenic area, respectively (Fig. 11), which indicates a mantle-derived magma source. These zircons mainly plot within the area of the rhyolites and away from those of the Emeishan basalts (Huang et al., 2022). Moreover, few zircons with core-rim structures and older concordant ages (>280 Ma) plot within the continental arc-related area, which suggests that they were inherited from the older crust. Combined with the temporal range, these features suggest that the zircons in the polymetallic beds were dominantly sourced from the Emeishan silicic rocks. These zircons thus provide Hf isotopes and trace elements of significance for deciphering the magmatic evolution of the eroded silicic rocks.

The minor Late Permian zircons from the Chahe section have negative εHf(*t*) values ranging from −10.1 to −0.5 (Fig. 12a), which correspond to Paleoproterozoic to Mesoproterozoic model ages (1.9–1.3 Ga). Meanwhile, these zircons have high Th/Nb (mostly >20) and U/Yb (mostly >0.6) ratios and exhibit continental arc-related features (Fig. 11). The negative εHf(*t*) values and trace elements of zircons reflect the contamination of preexisting lower crust in the source magma. Based on the trace element and εNd(*t*) value models, a crustal assimilation combined fractional crystallization (AFC) style was proposed for the genesis of the rhyolites in the Emeishan LIP inner zone (Xu et al., 2010; Usuki et al., 2015; Cheng et al., 2017; Hei et al., 2018). Moreover, these rhyolites are characterized by the εNd(*t*) values of −0.6 – +2.2 and mean zircon εHf(*t*) values of +5.5 – +6.5 (Usuki et al., 2015; Hei et al., 2018), which suggest minor crustal assimilation during the petrogenetic processes. Incidentally, the zircons from the rhyolites at the uppermost Shangcang section show low Th/Nb and U/Yb ratios and positive εHf(*t*) values (averages of +7.1 – +8.2), which imply that the silicic rocks in

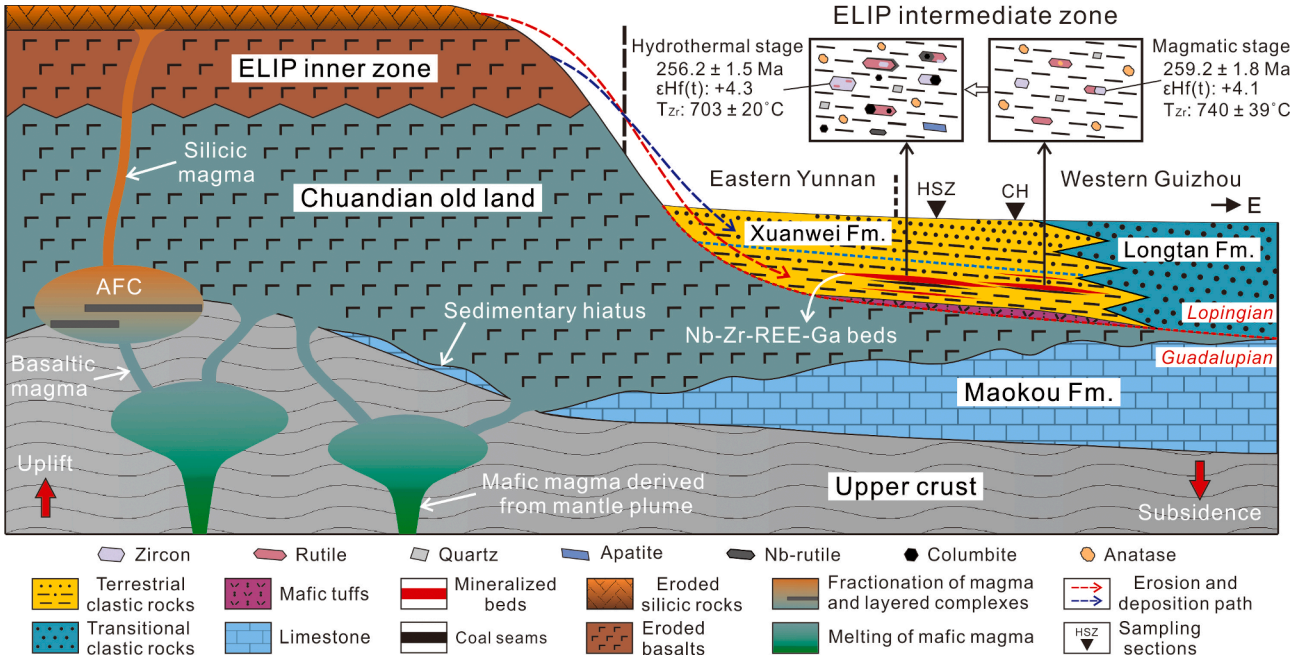

Fig. 14. Genetic model for Late Permian Nb-Zr-REE-Ga-enriched beds in western Guizhou Province. The eruption model of the central Emeishan LIP is modified after Shellnutt (2014).

the western Emeishan LIP were generated without significant crustal contamination (Huang et al., 2022). These zircon data are different from those of the Upper Permian strata in western Guizhou, which are proposed to source from silicic rocks in the central Emeishan LIP (Fig. 13; He et al., 2007; Xu et al., 2008; Yang et al., 2015; Deng et al., 2020). Given the zircon data of the clastic sediments and remnant rhyolites, the extrusive source rocks are proposed to have been generated from multistage silicic volcanisms with various degrees of crustal contamination.

Our data suggest that the zircons from older samples (ca. 259 Ma) show higher Th/Nb and U/Yb ratios and more negative εHf(*t*) values than those from the younger samples (ca. 256 Ma; Figs. 11, 12a). In addition, the early-stage zircons exhibit higher T_{Zr} and Eu/Eu* values, and smaller grain size than those of the late-stage zircons (Figs. 8, 10). These characteristics suggest that the early-stage magma with high temperatures tended to heat and melt the country rocks of the magma chamber. During the waning stage, the magma chamber could be replenished by parental magma and continuously evolved into a homogeneous system, which may have continued until middle Wuchiapingian. In addition, the εHf(*t*) values of the zircon in the lower Xuanwei Formation are comparable to those in the lower Shaiwa and Longtan formations (Fig. 12b; Yang et al., 2015; Deng et al., 2020). Together with the zircon data from the lowermost Xuanwei Formation (He et al., 2007; Xu et al., 2008), the zircons from the stratigraphic lower samples show higher εHf(*t*) values, lower Th/Nb and U/Yb ratios than the zircons from the upper samples (Fig. 13). The geochemical and isotopic variations in these zircons document a decrease in crustal contribution. Integrated with previous studies on the rhyolites and trachytes, the zircon data from the lower Xuanwei Formation suggest a fractional crystallization dominated petrogenetic process with diminished crustal assimilation for the eroded silicic rocks of the Emeishan LIP.

7. Conclusions

(1) Whole-rock major and trace geochemistry suggest that the Nb-Zr-REE-Ga enrichments in western Guizhou were dominantly derived from alkaline silicic rocks in the central Emeishan LIP. The barren samples show geochemical affinities with the underlying high-Ti basalts and mafic tuffs, and they have incorporated with basaltic compositions.
(2) Detrital zircons of the polymetallic beds yielded U−Pb ages of 259.2–256.2 Ma and εHf(*t*) values of −10.1 − +13.4, which are consistent with the zircon data of the alkaline rhyolites in the Emeishan LIP inner zone.
(3) The euhedral rutile coexisted with low-temperature zircon, and was replaced by Nb-rutile and columbite, which suggest that they were crystallized from an evolved alkaline magma and were likely to experience magmatic-hydrothermal processes.
(4) The temporal decreases of zircon Eu/Eu* values and crystallization temperatures indicate that the rare metals were concentrated during the protracted alkaline magmatism.
(5) The zircons from the older samples exhibit higher Th/Nb and U/Yb ratios, and more negative εHf(*t*) values than those from the younger samples, which suggest a magmatic evolution with decreasing crustal contamination for the generation of the eroded silicic rocks.

Declaration of Competing Interest

The authors declare that they have no known competing financial interests or personal relationships that could have appeared to influence the work reported in this paper.

Data availability

Data will be made available on request.

Acknowledgements

This research was supported by the National Key R&D Program of China (2017YFC0602500), National Natural Science Foundation of China (Grant Nos. 92162214, 41773015, and U1812402), and Key R&D Program of Yunnan Province (202103AQ100003). We thank editor, Prof. Huayong Chen for handling of the manuscript and two anonymous reviewers for their constructive comments.

Appendix A. Supplementary data

Supplementary data to this article can be found online at https://doi.org/10.1016/j.oregeorev.2022.105160.

References

Alves, M.A.d.S., Pereira, V.P., Neto, A.C.B., Menegotto, E., 2018. Weathering of the Madeira world-class Sn-Nb-Ta (Cryolite, REE, U, Th) deposit, Pitinga Mine (Amazon, Brazil). J. Geochem. Explor. 186, 61–76.
Arbuzov, S.I., Spears, D.A., Vergunov, A.V., Ilenok, S.S., Mezhibor, A.M., Ivanov, V.P., Zarubina, N.A., 2019. Geochemistry, mineralogy and genesis of rare metal (Nb-Ta-Zr-Hf-Y-REE-Ga) coals of the seam XI in the south of Kuznetsk Basin. Russia. Ore Geol. Rev. 113, 103073.
Belousova, E.A., Griffin, W.L., O'Reilly, S.Y., Fisher, N.I., 2002. Igneous zircon: trace element composition as an indicator of source rock type. Contrib. Mineral. Petr. 143, 602–622.
Blichert-Toft, J., Albarède, F., 1997. The Lu-Hf isotope geochemistry of chondrites and the evolution of the mantle-crust system. Earth Planet. Sci. Lett. 148, 243–258.
Burger, K., Zhou, Y.P., Tang, D.Z., 1990. Synsedimentary volcanic-ash-derived illite tonsteins in Late Permian coal-bearing formations of southwestern China. Int. J. Coal Geol. 15, 341–356.
Camden, R.H., Robert, L.S., 1988. RIR – Measurement and Use in Quantitative XRD. Powder Diffr. 3, 74–77.
Černý, P., Chapman, R., Göd, R., Niedermayr, G., Wise, M.A., 1989. Exsolution Intergrowths of Titanian Ferrocolumbite and Niobian Rutile from the Weinebene Spodumene Pegmatites, Carinthia. Austria. Miner. Petrol. 40, 197–206.
Cheng, L.L., Wang, Y., Herrin, J.S., Ren, Z.Y., Yang, Z.F., 2017. Origin of K-feldspar megacrysts in rhyolites from the Emeishan large igneous province, southwest China. Lithos 294–295, 397–411.
Chung, S.L., Jahn, B.M., Wu, G.Y., Lo, C.H., Cong, B.L., 1998. The Emeishan flood basalt in SW China: a mantle plume initiation model and its connection with continental break-up and mass extinction at the Permian–Triassic boundary. In: Flower, M.F.J., Chung, S.L., Lo, C.H., Lee, T.Y., (Eds.), Mantle Dynamics and Plate Interaction in East Asia: AGU Geodynamic Series. 27, pp. 47–58.
Chung, S.L., Jahn, B.M., 1995. Plume-lithosphere interaction in generation of the Emeishan flood basalts at the Permian-Triassic boundary. Geology 23, 889–892.
Dai, S.F., Zhou, Y.P., Zhang, M.Q., Wang, X.B., Wang, J.M., Song, X.L., Jiang, Y.F., Luo, Y.B., Song, Z., Yang, Z., Ren, D.Y., 2010. A new type of Nb(Ta)-Zr(Hf)-REE-Ga polymetallic deposit in the late Permian coal-bearing strata, eastern Yunnan, southwestern China: possible economic significance and genetic implications. Int. J. Coal Geol. 83, 55–63.
Dai, S.F., Li, T., Seredin, V.V., Ward, C.R., Hower, J.C., Zhou, Y.P., Zhang, M.Q., Song, X. L., Song, W.J., Zhao, C.L., 2014. Origin of minerals and elements in the Late Permian coals, tonsteins, and host rocks of the Xinde Mine, Xuanwei, eastern Yunnan. China. Int. J. Coal Geol. 121, 53–78.
Dai, S.F., Chekryzhov, I.Y., Seredin, V.V., Nechaev, V.P., Graham, I.T., Hower, J.C., Ward, C.R., Ren, D.Y., Wang, X.B., 2016a. Metalliferous coal deposits in East Asia (Primorye of Russia and South China): a review of geodynamic controls and styles of mineralization. Gondwana Res. 29, 60–82.
Dai, S.F., Liu, J.J., Ward, C.R., Hower, J.C., French, D., Jia, S.H., Hood, M.M., Garrison, T.M., 2016b. Mineralogical and geochemical compositions of Late Permian coals and host rocks from the Guxu Coalfield, Sichuan Province, China, with emphasis on enrichment of rare metals. Int. J. Coal Geol. 166, 71–95.
Dai, S.F., Nechaev, V.P., Chekryzhov, I.Y., Zhao, L.X., Vysotskiy, S.V., Graham, I.T., Ward, C.R., Ignatiev, A.V., Velivetskaya, T.A., Zhao, L., French, D., Hower, J.C., 2018. A model for Nb-Zr-REE-Ga enrichment in Lopingian altered alkaline volcanic ashes: Key evidence of H-O isotopes. Lithos 302–303, 359–369.
Deng, X.S., Yang, J.H., Cawood, P.A., Wang, X.C., Du, Y.S., Huang, Y., Lu, S.F., He, B., 2020. Detrital record of late-stage silicic volcanism in the Emeishan large igneous province. Gondwana Res. 79, 197–208.
DZ/T 0203-2020, 2020. Geology mineral industry standard of P.R. China: Specifications for rare metal mineral exploration. Geological Press, Beijing. (in Chinese).
Ferry, J.M., Watson, E.B., 2007. New thermodynamic models and revised calibrations for the Ti-in-zircon and Zr-in-rutile thermometers. Contrib. Mineral. Petr. 154, 429–437.
Griffin, W.L., Pearson, N.J., Belousova, E., Jackson, S.E., Van Achterbergh, E., O'Reilly, S.Y., Shee, S.R., 2000. The Hf isotope composition of cratonic mantle: LAM-MC-ICPMS analysis of zircon megacrysts in kimberlites. Geochim. Cosmochim. Acta 64, 133–147.
Grimes, C.B., Wooden, J.L., Cheadle, M.J., John, B.E., 2015. "Fingerprinting" tectono-magmatic provenance using trace elements in igneous zircon. Contrib. Mineral. Petr. 170, 1–26.

Hayashi, K., Fujisawa, H., Holland, H.D., Ohmoto, H., 1997. Geochemistry of ~1.9 Ga sedimentary rocks from northeastern Labrador. Canada. Geochim. Cosmochim. Acta 61, 4115–4137.
He, B., Xu, Y.G., Chung, S.L., Xiao, L., Wang, Y.M., 2003. Sedimentary evidence for a rapid, kilometer scale crustal doming prior to the eruption of the EFB. Earth Planet. Sci. Lett. 213, 391–405.
He, B., Xu, Y.G., Huang, X.L., Luo, Z.Y., Shi, Y.R., Yang, Q.J., Yu, S.Y., 2007. Age and duration of the Emeishan flood volcanism, SW China: Geochemistry and SHRIMP zircon U-Pb dating of silicic ignimbrites, post-volcanic Xuanwei Formation and clay tuff at the Chaotian section. Earth Planet. Sci. Lett. 255, 306–323.
He, B., Xu, Y.G., Zhong, Y.T., Guan, J.P., 2010. The Guadalupian-Lopingian boundary mudstones at Chaotian (SW China) are clastic rocks rather than acidic tuffs: implication for a temporal coincidence between the end-Guadalupian mass extinction and the Emeishan volcanism. Lithos 119, 10–19.
Hei, H.X., Su, S.G., Wang, Y., Mo, X.X., Luo, Z.H., Liu, W.G., 2018. Rhyolites in the Emeishan large igneous province (SW China) with implications for plume-related felsic magmatism. J. Asian Earth Sci. 164, 344–365.
Horbe, A.M.C., Costa, M.L.d., 1999. Geochemical evolution of a lateritic Sn–Zr–Th–Nb–Y–REE-bearing ore body derived from apogranite: the case of Pitinga, Amazonas — Brazil. J. Geochem. Explor. 66, 339–351.
Hoskin, P.W.O., Schaltegger, U., 2003. The composition of zircon and igneous and metamorphic petrogenesis. Rev. Mineral. Geochem. 53, 27–62.
Hu, Z.C., Liu, Y.S., Gao, S., Liu, W.G., Zhang, W., Tong, X.R., Lin, L., Zong, K.Q., Li, M., Chen, H.H., 2012. Improved in situ Hf isotope ratio analysis of zircon using newly designed X skimmer cone and jet sample cone in combination with the addition of nitrogen by laser ablation multiple collector ICP-MS. J. Anal. Atom. Spectrom. 27, 1391–1399.
Huang, X.H., 1997. The Lufang rare earth deposit in Weining, western Guizhou and its mineralization. Guizhou Geol. 14, 328–333 in Chinese with English abstract.
Huang, H., Cawood, P.A., Hou, M.C., Yang, J.H., Ni, S.J., Du, Y.S., Yan, Z.K., Wang, J., 2016. Silicic ash beds bracket Emeishan Large Igneous province to <1 m.y. at ~260 Ma. Lithos 264, 17–27.
Huang, H., Cawood, P.A., Hou, M.C., Ni, S.J., Yang, J.H., Du, Y.S., Wen, H.J., 2018. Provenance of Late Permian volcanic ash beds in South China: Implications for the age of Emeishan volcanism and its linkage to climate cooling. Lithos 314–315, 293–306.
Huang, H., Cawood, P.A., Hou, M.C., Xiong, F.H., Ni, S.J., Deng, M., Zhong, H.T., Yang, C.C., 2022. Zircon U-Pb age, trace element, and Hf isotopic constrains on the origin and evolution of the Emeishan Large Igneous Province. Gondwana Res. 105, 535–550.
Jackson, S.E., Pearson, N.J., Griffin, W.L., Belousova, E.A., 2004. The application of laser ablation-inductively coupled plasma-mass spectrometry to in situ U-Pb zircon geochronology. Chem. Geol. 211, 47–69.
Lazareva, E.V., Zhmodik, S.M., Dobretsov, N.L., Tolstov, A.V., Shcherbov, B.L., Karmanov, N.S., Gerasimov, E.Y., Bryanskaya, A.V., 2015. Main minerals of abnormally high-grade ores of the Tomtor deposit (Arctic Siberia). Russ. Geol. Geophys. 56, 844–873.
Li, H.B., Zhang, Z.C., Santosh, M., Lü, L.S., Han, L., Liu, W., 2017. Late Permian basalts in the Yanghe area, eastern Sichuan Province, SW China: Implications for the geodynamics of the Emeishan flood basalt province and Permian global mass extinction. J. Asian Earth Sci. 134, 293–308.
Liu, Y.S., Hu, Z.C., Gao, S., Günther, D., Xu, J., Gao, C.G., Chen, H.H., 2008. In situ analysis of major and trace elements of anhydrous minerals by LA-ICP-MS without applying an internal standard. Chem. Geol. 257, 34–43.
Liu, Y.S., Gao, S., Hu, Z.C., Gao, C.G., Zong, K.Q., Wang, D.B., 2010. Continental and oceanic crust recycling-induced melt-peridotite interactions in the Trans-North China Orogen: U-Pb dating, Hf isotopes and trace elements in zircons of mantle xenoliths. J. Petrol. 51, 537–571.
Liu, X.J., Liang, Q.D., Li, Z.L., Castillo, P.R., Shi, Y., Xu, J.F., Huang, X.L., Liao, S., Huang, W.L., Wu, W.N., 2017. Origin of Permian extremely high Ti/Y mafic lavas and dykes from Western Guangxi, SW China: Implications for the Emeishan mantle plume magmatism. J. Asian Earth Sci. 141, 97–111.
Liu, J.J., Song, H.J., Dai, S.F., Nechaev, V.P., Graham, I.T., French, D., Nechaeva, E.V., 2019. Mineralization of REE-Y-Nb-Ta-Zr-Hf in Wuchiapingian coals from the Liupanshui Coalfield, Guizhou, southwestern China: geochemical evidence for terrigenous input. Ore Geol. Rev. 115, 103190.
Ludwig, K.R., 2003. ISOPLOT 3.00: A Geochronological Toolkit for Microsoft Excel. Berkeley Geochronology Center, California, Berkeley, p. 39.
McLennan, S.M., Hemming, S., McDaniel, D.K., Hanson, G.N. 1993. Geochemical approaches to sedimentation, provenance, and tectonics, in: Johnsson, M.J., Basu, A. (Eds.), Processes controlling the composition of clastic sediments. Geological Society of America Special Paper. 284. 21–40.
Meinhold, G., 2010. Rutile and its applications in earth sciences. Earth Sci. Rev. 102, 1–28.
Meng, C.Z., Chen, Y., Zhang, Y.H., Wu, H., Ling, W.L., Zhang, H., Liu, J., 2015. Genetic relationship between unroofing of the Emeishan large igneous province and the iron-polymetallic deposit in western Guizhou, Southwestern China: Constraint from U-Pb geochronology and geochemistry of zircon. Sci. China Earth Sci. 58, 1939–1950.
Morel, M.L., Nebel, O., Nebel-Jacobsen, Y.J., Miller, J.S., Vroon, P.Z., 2008. Hafnium isotope characterization of the GJ-1 zircon reference material by solution and laser-ablation MC-ICPMS. Chem. Geol. 255, 231–235.
Mundil, R., Ludwig, K.R., Metcalfe, I., Renne, P.R., 2004. Age and timing of the Permian mass extinctions: U/Pb dating of closed-system zircons. Science 305, 1760–1763.
Nesbitt, H.W., Young, G.M., 1982. Early Proterozoic climates and plate motions inferred from major element chemistry of lutites. Nature 299, 715–717.
Seredin, V.V., Dai, S.F., 2012. Coal deposits as potential alternative sources for lanthanides and yttrium. Int. J. Coal Geol. 94, 67–93.
Seredin, V.V., Finkelman, R.B., 2008. Metalliferous coals: a review of the main genetic and geochemical types. Int. J. Coal Geol. 76, 253–289.
Shellnutt, J.G., 2014. The Emeishan large igneous province: A synthesis. Geosci. Front. 5, 369–394.
Shellnutt, J.G., Jahn, B.-M., 2010. Formation of the Late Permian Panzhihua plutonic-hypabyssal-volcanic igneous complex: Implications for the genesis of Fe-Ti oxide deposits and A-type granites of SW China. Earth Planet. Sci. Lett. 289, 509–519.
Shellnutt, J.G., Pham, T.T., Denyszyn, S.W., Yeh, M.W., Tran, T.A., 2020. Magmatic duration of the Emeishan large igneous province: Insight from northern Vietnam. Geology 48, 457–461.
Shen, S.Z., Crowley, J.L., Wang, Y., Bowring, S.A., Erwin, D.H., Sadler, P.M., Cao, C.Q., Rothman, D.H., Henderson, C.M., Ramezani, J., Zhang, H., Shen, Y.N., Wang, X.D., Wang, W., Mu, L., Li, W.Z., Tang, Y.G., Liu, X.L., Liu, L.J., Zeng, Y., Jiang, Y.F., Jin, Y.G., 2011. Calibrating the end-Permian mass extinction. Science 334, 1367–1372.
Shen, M.L., Dai, S.F., Graham, I.T., Nechaev, V.P., French, D., Zhao, F.H., Shao, L.Y., Liu, S.D., Zuo, J.P., Zhao, J.T., Chen, K., Xie, X.H., 2021. Mineralogical and geochemical characteristics of altered volcanic ashes (tonsteins and K-bentonites) from the latest Permian coal-bearing strata of western Guizhou Province, southwestern China. Int. J. Coal Geol. 237, 103707.
Söderlund, U., Patchett, P.J., Vervoort, J.D., Isachsen, C.E., 2004. The Lu-176 decay constant determined by Lu-Hf and U-Pb isotope systematics of Precambrian mafic intrusions. Earth Planet. Sci. Lett. 219, 311–324.
Sun, S.-S., McDonough, W.F., 1989. Chemical and isotopic systematics of oceanic basalts: Implications for mantle composition and processes. Geol. Soc. Lond. Spec. Publ. 42, 313–345.
Taylor, S.R., McLennan, S.M., 1985. The Continental Crust: Its Composition and Evolution. Blackwell, Oxford, p. 312.
Usuki, T., Lan, C.Y., Tran, T.H., Pham, T.D., Wang, K.L., Shellnutt, J.G., Chung, S.L., 2015. Zircon U-Pb ages and Hf isotopic compositions of alkaline silicic magmatic rocks in the Phan Si Pan–Tu Le region, northern Vietnam: Identification of a displaced western extension of the Emeishan large igneous province. J. Asian Earth Sci. 97, 102–124.
Vervoort, J.D., Blichert-Toft, J., 1999. Evolution of the depleted mantle: Hf isotope evidence from juvenile rocks through time. Geochim. Cosmochim. Acta 63, 533–556.
Wang, N., Dai, S.F., Wang, X.B., Nechaev, V.P., French, D., Graham, I.T., Zhao, L., Song, X.L., 2022. New insights into the origin of Middle to Late Permian volcaniclastics (Nb-Zr-REY-Ga-rich horizons) from eastern Yunnan. SW China. Lithos 420–421, 106702.
Wang, X.T., Shao, L.Y., Eriksson, K.A., Yan, Z.M., Wang, J.M., Li, H., Zhou, R.X., Lu, J., 2020. Evolution of a plume-influenced source-to-sink system: An example from the coupled central Emeishan large igneous province and adjacent western Yangtze cratonic basin in the Late Permian. SW China. Earth Sci. Rev. 207, 103224.
Wang, F.L., Zhao, T.P., Chen, W.T., Wang, C.Y., 2013. Zircon U-Pb ages and Lu-Hf isotopic compositions of the Nb-Ta-Zr-bearing syenitic dikes in the Emeishan large igneous province. Acta Petrol. Sin. 29, 3519–3532 in Chinese with English abstract.
Wang, F.L., Wang, C.Y., Zhao, T.P., 2015. Boron isotopic constraints on the Nb and Ta mineralization of the syenitic dikes in the ~260 Ma Emeishan large igneous province (SW China). Ore Geol. Rev. 65, 1110–1126.
Wang, S.Y., Yin, H.F., 2001. Study in Terrestrial Permian-Triassic Boundary in Eastern Yunnan and Western Guizhou. China University of Geoscience Press, Wuhan (in Chinese with English abstract).
Wiedenbeck, M., Alle, P., Corfu, F., Griffin, W.L., Meier, M., Oberli, F.V., Quadt, A.V., Roddick, J.C., Spiegel, W., 1995. Three natural zircon standards for U-Th-Pb, Lu-Hf, trace element and REE analyses. Geostand. Geoanal. Res. 19, 1–23.
Winchester, J.A., Floyd, P.A., 1977. Geochemical discrimination of different magma series and their differentiation products using immobile elements. Chem. Geol. 20, 325–343.
Woodhead, J., Hergt, J., Shelley, M., Eggins, S., Kemp, R., 2004. Zircon Hf-isotope analysis with an excimer laser, depth profiling, ablation of complex geometries, and concomitant age estimation. Chem. Geol. 209, 121–135.
Xiao, L., Xu, Y.G., Mei, H.J., Zheng, Y.F., He, B., Pirajno, F., 2004. Distinct mantle sources of low-Ti and high-Ti basalts from the western Emeishan large igneous province, SW China: Implications for plume-lithosphere interaction. Earth Planet. Sci. Lett. 228, 525–546.
Xu, Y.G., Chung, S.L., Jahn, B.M., Wu, G.Y., 2001. Petrologic and geochemical constraints on the petrogenesis of Permian-Triassic Emeishan flood basalts in southwestern China. Lithos 58, 145–168.
Xu, Y.G., He, B., Chung, S.L., Menzies, M.A., Frey, F.A., 2004. Geologic, geochemical, and geophysical consequences of plume involvement in the Emeishan flood-basalt province. Geology 32, 917–920.
Xu, Y.G., Luo, Z.Y., Huang, X.L., He, B., Xiao, L., Xie, L.W., Shi, Y.R., 2008. Zircon U-Pb and Hf isotope constraints on crustal melting associated with the Emeishan mantle plume. Geochim. Cosmochim. Acta 72, 3084–3104.
Xu, Y.G., Chung, S.L., Shao, H., He, B., 2010. Silicic magmas from the Emeishan large igneous province, Southwest China: Petrogenesis and their link with the end-Guadalupian biological crisis. Lithos 119, 47–60.
Yang, J.H., Cawood, P.A., Du, Y.S., Huang, H., Huang, H.W., Tao, P., 2012. Large Igneous Province and magmatic arc sourced Permian-Triassic volcanogenic sediments in China. Sediment. Geol. 261–262, 120–131.
Yang, J.H., Cawood, P.A., Du, Y.S., Huang, H., Hu, L.S., 2014. A sedimentary archive of tectonic switching from Emeishan Plume to Indosinian orogenic sources in SW China. J. Geol. Soc. London 171, 269–280.

Yang, J.H., Cawood, P.A., Du, Y.S., 2015. Voluminous silicic eruptions during late Permian Emeishan igneous province and link to climate cooling. Earth Planet. Sci. Lett. 432, 166–175.
Yang, J.H., Cawood, P.A., Du, Y.S., Condon, D.J., Yan, J.X., Liu, J.Z., Huang, Y., Yuan, D. X., 2018. Early Wuchiapingian cooling linked to Emeishan basaltic weathering? Earth Planet. Sci. Lett. 492, 102–111.
Yang, R.D., Wang, W., Zhang, X.D., Liu, L., Wei, H.R., Bao, M., Wang, J.X., 2008. A new type of rare earth elements deposit in weathering crust of Permian basalt in western Guizhou. NW China. J. Rare Earth. 26, 753–759.
Yu, W.C., Algeo, T.J., Du, Y.S., Zhang, Q.L., Liang, Y.P., 2016. Mixed volcanogenic–lithogenic sources for Permian bauxite deposits in southwestern Youjiang Basin, South China, and their metallogenic significance. Sediment. Geol. 341, 276–288.
Zeng, Z.Y., Liu, Y., 2022. Magmatic–hydrothermal zircons in syenite: A record of Nb–Ta mineralization processes in the Emeishan large igneous province. SW China. Chem. Geol. 589, 120675.
Zhang, Z.W., Yang, X.Y., Li, S., Zhang, Z.S., 2010. Geochemical characteristics of the Xuanwei Formation in West Guizhou: Significance of sedimentary environment and mineralization. Chinese J. Geochem. 29, 355–364.
Zhang, Z.W., Zheng, G.D., Takahashi, Y., Wu, C.Q., Zheng, C.F., Yao, J.H., Xiao, C.Y., 2016. Extreme enrichment of rare earth elements in hard clay rocks and its potential as a resource. Ore Geol. Rev. 72, 191–212.
Zhao, L.X., Dai, S.F., Graham, I.T., Li, X., Zhang, B.B., 2016. New insights into the lowest Xuanwei Formation in eastern Yunnan Province, SW China: Implications for Emeishan large igneous province felsic tuff deposition and the cause of the end-Guadalupian mass extinction. Lithos 264, 375–391.
Zhao, L.X., Dai, S.F., Graham, I.T., Li, X., Liu, H.D., Song, X.L., Hower, J.C., Zhou, Y.P., 2017. Cryptic sediment-hosted critical element mineralization from eastern Yunnan Province, southwestern China: mineralogy, geochemistry, relationship to Emeishan alkaline magmatism and possible origin. Ore Geol. Rev. 80, 116–140.
Zhao, L., Dai, S.F., Nechaev, V.P., Nechaeva, E.V., Graham, I.T., French, D., Sun, J.H., 2019. Enrichment of critical elements (Nb-Ta-Zr-Hf-REE) within coal and host rocks from the Datanhao mine, Daqingshan Coalfield, northern China. Ore Geol. Rev. 111, 102951.
Zhong, Y.T., He, B., Mundil, R., Xu, Y.G., 2014. CA-TIMS zircon U-Pb dating of felsic ignimbrite from the Binchuan section: Implications for the termination age of Emeishan large igneous province. Lithos 204, 14–19.
Zhong, Y.T., Mundil, R., Chen, J., Yuan, D.X., Denyszyn, S.W., Jost, A.B., Payne, J.L., He, B., Shen, S.Z., Xu, Y.G., 2020. Geochemical, biostratigraphic, and high-resolution geochronological constraints on the waning stage of Emeishan Large Igneous Province. GSA Bull. 132, 1969–1986.
Zhou, Y.P., Ren, Y.L., Bohor, B.F., 1982. Origin and distribution of tonsteins in Late Permian coal seams of southwestern China. Int. J. Coal Geol. 2, 49–77.
Zhou, Y.P., Bohor, B.F., Ren, Y.L., 2000. Trace element geochemistry of altered volcanic ash layers (tonsteins) in late Permian coal-bearing formations of Eastern Yunnan and Western Guizhou Province. China. Int. J. Coal Geol. 44, 305–324.
Zhou, L.J., Zhang, Z.W., Li, Y.J., You, F.H., Wu, C.Q., Zheng, C.F., 2013. Geological and geochemical characteristics in the paleo-weathering crust sedimentary type REE deposits, western Guizhou. China. J. Asian Earth Sci. 73, 184–198.